7-8-2009

Synthesis, characterization and fluorescence performance of LaF3:Ce3+ nanocrystals

Fan Yang

Follow this and additional works at: https://digitalrepository.unm.edu/me_etds

Fan Yang

Candidate

Mechanical Engineering

Department

This thesis is approved, and it is acceptable in quality
and form for publication:

Approved by the Thesis Committee:

_____ ,Chairperson

Zayd Chad Leseman   March 6, 2009

Clau Clulus   March 06, 2009.

_____

_____

_____

_____

_____

**SYNTHESIS, CHARACTERIZATION AND FLUORESCENCE
PERFORMANCE OF LAF3:CE3+ NANOCRYSTALS**

BY

FAN YANG

B.S., SICHUAN UNIVERSITY, 2002

THESIS

Submitted in Partial Fulfillment of the
Requirements for the Degree of

Master of Science in Mechanical Engineering

The University of New Mexico
Albuquerque, New Mexico

May, 2009

Dedication

I would like to express my deepest love and gratitude to my family. Thanks to my parents who encourage me to pursue best education. Thanks to my younger brother, for all the support and happiness he brought to me. Especially, I would like to thank my best friend, my true love, and my husband, Jian, for being with me with unconditional support and love.

Acknowledgements

I would like to take this opportunity to express my sincere thanks to my advisor, Professor Al-Haik, for providing me an environment with great freedom in the group, for his insightful ideas to direct my graduate research, and for his encouragements, kind favors and supports in my life.

I would like to thank all members of my committee. Thanks to Dr. Luhrs and Dr. Leseman for all the discussions and time. Special appreciations to Dr. Luhrs for her patient help when I began to work on the nanocrystals project, for her creative ideas directing my project as well as generously teaching me to use all experimental facilities related to my research. The Laboratory of Functional Nanomaterials at the Mechanical Engineering in UNM is a great place to work in, and I enjoyed every day working with a group of brilliant people there. I thank Dr. Cabaniss and Dr. Stephen Ho for their help in using their Spectrophotometer and in solving technical problems I met. My thanks go to the materials group members: Stephen, Juanita, Mehran, Mark, Korbie for helping me in taking SEM and TEM images that I used in my thesis.

Also, I want to express my gratitude to my friends. Thanks to Zhijun Zhou, Yanli Tang and Yongqian Gao for their help in fluorescence testing. Especially, I would like to thank my other three good friends, Guanlin Tang, Shuangwei Xie and Chengao Wang, for their support and for everything they have done for me.

SYNTHESIS, CHARACTERIZATION AND FLUORESCENCE PERFORMANCE OF LAF3: CE3+ NANOCRYSTALS

BY

FAN YANG

ABSTRACT OF THESIS

Submitted in Partial Fulfillment of the
Requirements for the Degree of

Master of Science in Mechanical Engineering

The University of New Mexico
Albuquerque, New Mexico

May, 2009

Synthesis, Characterization and Fluorescence Performance of LaF$_3$: Ce^{3+} Nanocrystals

by

Fan Yang

B.S., Sichuan University, 2002

Master, Mechanical Engineering, UNM, 2009

ABSTRACT

Fluorescent labeling agents have greatly affected many biological applications in recent years. Among different types of labeling agents, Cerium-doped LaF$_3$ nanocrystals (NCs) are considered to be a promising new class of luminescent materials. Usually, lanthanide-doped nanocrystals production entails the use of ligands and high-temperature, which limits their biological applications and lowers their processability. This thesis proposes a simple and affordable synthesis of water-soluble LaF$_3$: Ce doped nanocrystals without using ligands and at low temperatures. Dispersion of the nanoparticles was carried out in three different solvents including methanol, distilled-water and DI-chitosan. The effects of different levels of dopant on the particle size, morphology and their luminescent properties were investigated. Parametric performance of the synthesized materials was investigated in light of several parameters: different Ce concentrations, different solvents and different fluorophores concentrations as well. In general higher fluorophores concentration dispersed in DI- water solvent yielded better emission and better quantum efficiency.

Contents

List of Figures

List of Tables

Chapter 1

Introduction

Nanoparticles with good fluorescence properties have attracted growing attentions in recent years. It is not only because they are considered as useful active components in lamps, displays (Stryganyuk et al. 2007), optical amplifiers (Hui et al. 2007), but also because lanthanide doped nanocrystals recently have been widely used for a variety of biological applications (Zhang et al. 2007; Meyssamy et al. 1999).

In medical and biochemical research, organic fluorescent compounds are extensively used as optical markers for proteins or nucleic acids in the study of molecular and cellular processes (Stryganyuk et al. 2007). Quantum dots have been used as fluorescent labels (Stouwdam et al. 2003) and have already led to very promising results (Cooke et al. 2006). However, a major drawback of Cd (S, Se) or InP quantum dots is their high toxicity, which hinders their usage at *in vivo* applications. At *in vitro* applications,

quantum dots are often hampered by their complex water solubility and their fluorescence intermittency (Stouwdam and Veggel 2002).

Recently, lanthanide ion-doped oxide nanoparticles have been proposed as biological fluorescent labels (Stouwdam et al. 2003), since they exhibit strong fluorescence and large Stokes shifts[1]. Typically the emission spectrum of such materials is characterized by narrow emission bandwidths independent of their particle size, and their colloidal synthesis is well described. Moreover, they exhibit long luminescence lifetimes, which enables time-sensitive detection.

Compared to classical luminescent materials, fluorides are more advantageous for several reasons. Fluorides have low vibrational energies that subsequently will minimize the quenching of the excited state of the rare earth ion (e.g. Ce^{3+}) (Wang et al. 2006 Chem. Mater.). Fluorides also exhibit sufficient thermal and environmental stabilities. Rare earth fluorides have been utilized in several applications such as lighting and displays, photo electronics, biological labels, and optical amplifies (Justel et al. 1998).

Several synthesis techniques have been carried out for rare earth fluorides such as thermoanalysis of organometallic precursors in surfactant solutions (Liu et al. 2007). Alternatively, synthetic methods using ligands have been reported for LaF_3 (Stouwdam, et al. 2003; Stouwdam and Veggel 2004).

---

[1] Stokes shift represent the energy loss between excitation and emission spectra of fluorescent molecules, typically in solutions, due to both energy relaxation of the excited electrons and due to energy losses to the surrounding through the solution.

Thesis Objective:

The objective of this thesis is to investigate a simple and affordable synthesis route for cerium-doped lanthanum fluoride (LaF$_3$) nanoparticles with uniform size and shape which are soluble in organic solvents for tunable optical properties. The method utilized in this thesis and described herein does not require usage of ligands and produces LaF$_3$: Ce doped nanoparticles that can be well-dispersed and deagglomerated in water and/or organic solvents to form transparent colloidal solutions. Starting with lanthanide chlorides and ammonium fluoride in methanol solutions, a substitution reaction renders cerium doped lanthanum fluoride nanoparticles. Nanocrystals of LaF$_3$ with 0%, 1%, 5%, and 10% Ce were obtained by this route. The current thesis provides investigation of the fluorescence performance of LaF$_3$: Ce nanocrystals based on the following parameters: different Ce dopant concentrations, usage of DI- water solvent and DI- chitosan deagglomerater in the synthesis of LaF$_3$: Ce nanocrystals and concentrations of the LaF$_3$: Ce nanocrystals in different solutions.

1.1 Light interactions with solids

If a solid sample is illuminated by a light beam of certain intensity, in general, the intensity of the transmitted beam is lower than that of the incident beam. Several processes can contribute to this attenuation such as:

- *Absorption*, if the beam frequency is resonant with a ground to excited state transition of the atoms in the solid. A fraction of this intensity is generally emitted

at a lower frequency than that of the incident beam, giving rise to the emission intensity. The reminant of the absorbed intensity is lost through nonradiative processes (heat).

- *Reflection* with a different intensity from the external and internal surfaces.

- *Scattering*, with a light spread in several directions, due to elastic (at the same frequency as the incident beam) or inelastic (at lower and higher frequencies than that of the incident beam – Raman scattering) processes.

Optical spectroscopy analyzes frequencies and intensities of these emerging beams as a function of frequency and intensity of the incident beam.

1.2 *What are luminescence, fluorescence and photoluminescence?*

The word *luminescence*, including both fluorescence and phosphorescence, originates from the Latin word *lumen*, which means light. In spectroscopy the word *luminescence* is defined as a phenomenon in which the electronic state of a substance is excited by external energy stimulus and the excitation energy is given off as light. Here, the *light* includes not only electromagnetic waves in the visible region of 400 to 750 nm, but also those in the neighboring regions on both ends, i.e., near-ultraviolet (UV) and near-infrared (IR) regions (Weber 1967).

The visible light emission from a substance during the time when it is exposed to exciting radiation is called *fluorescence*, while the after-glow if detectable by the human eye after the cessation of excitation is called *phosphorescence*.

In excited singlet states, the electron in the excited orbital is paired (by opposite spin) to the second electron in the ground-state orbital. Consequently, return to the ground state is spin allowed and occurs rapidly by emission of a photon. The typical fluorescence lifetime is near 10 ns (10 x 10^{-9} s) (Lakowicz 2006).

Phosphorescence is the emission of light from triplet-excited states, in which an electron in the excited orbital has the same spin orientation as the ground-state electron. Transitions to the ground state are forbidden and the emission rates are slow so that phosphorescence lifetimes are typically milliseconds to seconds (Klink et al. 1999).

Photoluminescence occurs after excitation with light (i.e., radiation within the optical range). Luminescence can also be produced under excitation with an electron beam, and in this case it is called *cathodoluminescence*. This technique is conventionally used to investigate some characteristics of specimens, such as trace impurities and lattice defects, as well as to investigate crystal distortion. Excitation by high-energy electromagnetic radiation (sometimes called ionizing radiation) such as X-rays, *α*-rays (helium nuclei), *β*-rays (electrons), or *γ* -rays leads to a type of photoluminescence called *radioluminescence* (Valeur 2002).

Thermoluminescence occurs when a substance emits light as a result of the release of energy stored in traps by thermal heating. This mechanism is different from thermally produced blackbody radiation. *Electroluminescence* occurs as a result of the passage of an electric current through a material, as in nightlight panels.

Triboluminescence is the production of light by a mechanical disturbance, for instance, light that emerges when some adhesive tapes are unrolled. Acoustic waves (sound) passing through a liquid can produce *sonoluminescence*. *Chemiluminescence* appears as a result of a chemical reaction. As a particular class of chemiluminescence, *bioluminescence* occurs as a result of chemical reactions inside a biological organism. Fig 1.1 provides the classification of the different types of luminescence.
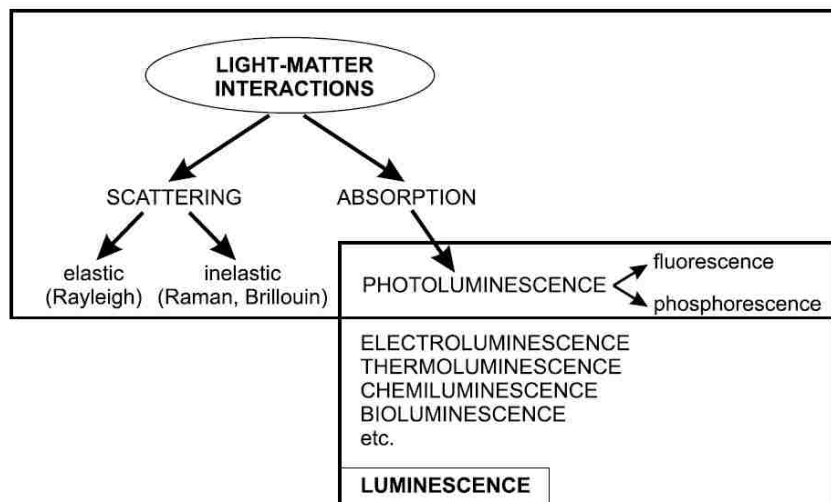
Fig1. 1 Various types of luminescence with corresponding excitation (Valeur 2002)

Fluorescence occurs when an atom, molecule or solid absorbs light photons from the UV-visible light spectrum, known as excitation, and then rapidly emits light photons as it

6

returns to its *ground state*; the state of lowest energy of that electron, thus it is given more energy and convert to a higher electronic energy state what is called "excited state" (Fig 1.2). In the excited state, an electron will not stay there too long since it is not stable, then the electron gives back the energy in the form of light and return to its ground state (Kitai 1993). (Fig 1.3)
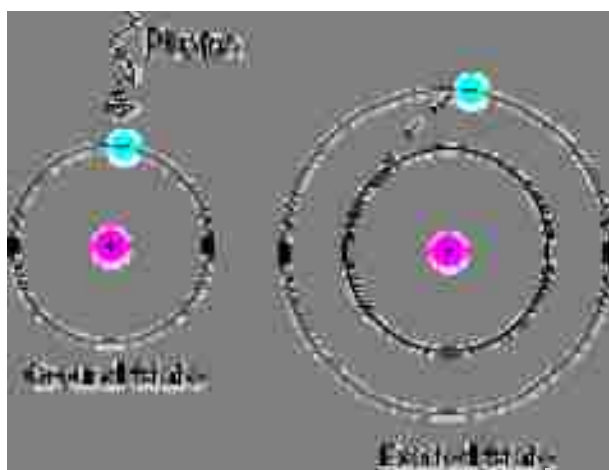
Fig 1.2 An electron becomes excited when it absorbs a photon (NASA Space Flight Center).
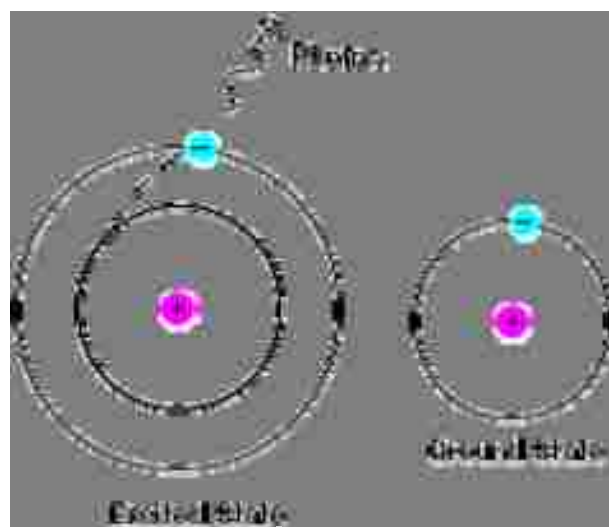
Fig 1.3 An electron goes back to ground state when it emits a photon (NASA Space Flight Center).

Fluorimetry characterizes the relationship between absorbed and emitted photons at specified wavelengths. It is a precise, quantitative, and analytical technique that is inexpensive and easily mastered. All chemical compounds absorb energy which causes excitation of electrons bound in the molecule, such as increased vibrational energy or, under appropriate conditions, transitions between discrete electronic energy states. For a transition to occur, the absorbed energy must be equivalent to the difference between the initial electronic state and a high-energy state. This value is constant and characteristic of the molecular structure. This is termed the excitation wavelength. If conditions permit, an excited molecule will return to its ground state by emission of energy through heat and/or emission of energy quanta such as photons.

Fluorescent compounds or *fluorophores* can be identified and quantified on the basis of their excitation and emission properties. The excitation spectra are determined by measuring the emission intensity at a fixed wavelength, while varying the excitation wavelength. The emission spectra are determined by measuring the variation in emission intensity wavelength for a fixed excitation wavelength (Lakowicz 2006).

During the excited-state lifetime, typically 1-10 nanoseconds, the fluorophore energy S_1' is dissipated and converts to a lower energy excited state S_1 where fluorescence emission originates. That means not all absorbed energy converts to fluorescence emission when electrons return to ground state (Kitai 1993). The vibrational energy loss results in an emission spectrum with longer wavelengths compared to the absorption/excitation spectrum is represented by C ($h\nu_{ex} - h\nu_{em}$) which is known as Stokes shift, where *h* is

8

Planck's constant and ν is the frequency of light. Therefore emitted photons have longer wavelengths than excited photons.

If S_1' denotes an excited state of a substance S_0, then fluorescence consists of the excitation: $S_0 + h\nu_{ex} \rightarrow S_1'$ and emission: $S_1 \rightarrow h\nu_{em} + S_0$. Generally speaking, the absorbed photon is in the UV range, and the emitted light is in the visible range.
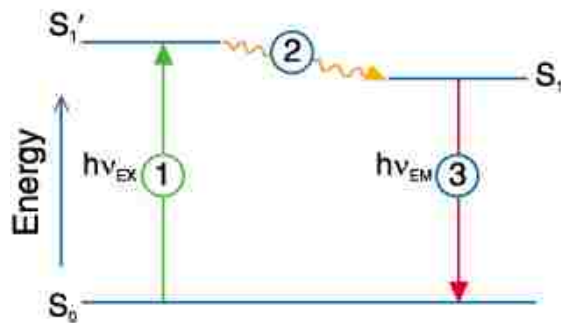
Fig 1. 4 A diagram illustrating the processes of excitation and emission of fluorescence (Invitrogens).

Quantum yield is the percentage of molecules in an excited electronic state that decay to ground state by fluorescent emission, i.e., rapid emission of a light photon in the range of 200- 900 nm. This value is always less than or equal to unity and is characteristic of the molecular structure.

Several factors contribute to the decay of the fluorophores and thus, reduce the fluorescence intensity and the quantum yield. In general, decay processes can be classified as: internal or external conversions (So and Dong 2002). Internal conversion is a process at which the electron energy is converted to vibrational energy of the fluorophore itself. Since vibrational processes are driven by thermal processes, the

internal conversion rate typically increases with temperature, which accounts for the commonly observed decrease in fluorescence intensity with rising temperature. External conversion describes the process where the fluorophore loses electronic energy to its environment through collision with other solutes. Upon collision, the fluorophore is de-excited nonradiatively. A number of important solute ions, such as oxygen, are efficient *fluorescence quenchers*. Usually, a fluorophore can be chemically bound to a quencher to form a 'dark complex' – a product that does not fluoresce (So and Dong 2002).

1.3 Types of fluorescence labeling materials

Commonly, there are three types of florescence labeling materials: quantum dots (QDs), organic dyes, and fluorescent nanoparticles (NPs) (Wang et al. 2006 Nanotech.). Organic dyes have inherent drawbacks such as susceptibility to chemical and photochemical degradation (Kumar 2000), decomposition under repeated excitation, and photochemical instabilities (Miyazaki et al. 1981). Compared to organic dyes, QDs are relatively more photochemically stable. They have been observed to have much higher luminescence efficiencies compared to nanoparticles based on sulphides, selenides, or tellurides of zinc and cadmium (Tian et al. 1996; Porteanu et al. 2001). Moreover, QDs have narrow emission bandwidths, size-dependent emissions, and high quantum yields (Medintz et al. 2005), which lead to successful applications in some biological analysis. However, some limitations of QDs exist as well, such as poor stability against oxidation, chemical instability, and optical blinking (Wang et al. 2006 Phys. Lett.; Wang et al. 2006 J. Mater. Chem.). These limitations make them unsuitable for high sensitivity quantitative bioassay.

Furthermore, these materials have inherent toxicity and inherent short luminescent lifetimes which make biological application difficult (Wang et al. 2006 Nanotech).

1.4 Fluorescent nanoparticles

Investigators have synthesized and observed the optical behavior of nanoparticles, motivated by their intriguing optical properties based on the premise of fewer defects at a reduced dimensionality in insulators, and the successful application of rare-earth doped nanocrystals (NCs) to radiation detection, mainly as gamma rays scintillators (Jiang et al. 2004).

Recently, emphasis has been placed on investigating the effect of reduced size on the luminescent properties of nanophosphors compared to their corresponding bulk materials (Cooke et al. 2006; McKigney et al. 2007). Bhargava et al. (1994), reported that the luminescence efficiency of surface-modified ZnS: Mn^{2+} nanophosphor increased with the decrease of particle size. The high-efficiency ZnS: Mn^{2+} nanophosphor has been explained via the following hypothesis: there is a strong coupling between ZnS s–p electron and Mn^{2+} d electron in the nanophosphor by quantum effect. Bhargava claimed that the hypothesis was supported by observation of shorter luminescence lifetime (3.7 ns and 20.5 ns) of nanophosphor than the bulk one (1.8 ms).

More recently, Cooker et al. (2006), have reported the reduced dimensional behavior of hydrothermally prepared Y_2SiO_5: Ce nanophosphors and their luminescent properties.

McKigney et al.(2007), reported radiation detection and nuclear spectroscopy of nanocomposite scintillators, comparing them with bulk-based scintillators. They found that, relative to bulk powder from which they were derived, the nanocomposite materials had improved properties which included enhanced light output, reduced cost, greater size scalability, and medium-dependent radiative lifetime.

1.5 Lanthanide-doped nanoparticles

Lanthanides, the name comes from *lanthanum,* are a series of fifteen metal elements from atomic number 57 through 71 in the periodic table. Pure lanthanides are silvery metals as shown in Fig 1.5.
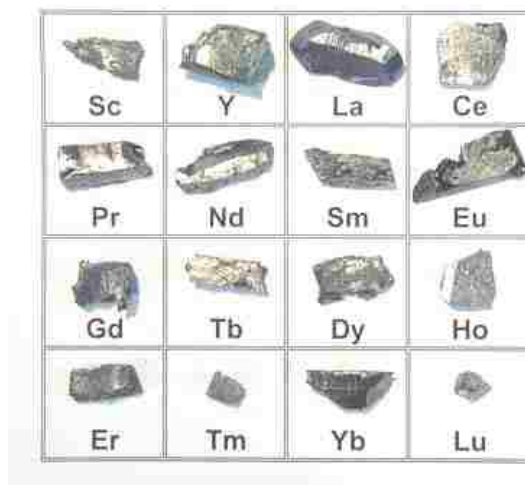
Fig 1.5 Pure Lanthanides are silvery metals (Metallium).

The name of the series comes from the earliest discovered element in the group: lanthanum (No 57), alternatively they are referred to as "rare earth elements" (Beatty 2007).

Lanthanide-doped nanocrystals emerged as a promising new class of biological fluorescent labels as alternatives to organic fluorophores and quantum dots, based on the their low toxicity (Beaurepaire et al. 2004). Moreover, the ease of extending the spectroscopic selectivity and manipulating the colors of lanthanide-doped nanocrystals (by using different lanthanide ions dopants) leads to extensive use in several bio applications. Moreover, they have long-lived luminescent lifetimes and high photochemical stability (Wang et al. 2006 Nanotech.).

In the current investigation, water-soluble lanthanide-based nanocrystals have been synthesized by a simple method at low temperature. Their shapes, sizes, structures and luminescent properties were carefully investigated as will be presented in following chapters of this thesis.

Chapter 2

Synthesis of nanocrystals

2.1 Lanthanide-based nanocrystals synthesis methods

Many techniques have been used to synthesize lanthanide-based nanocrystals. Usually, researchers made lanthanide-doped nanocrystals at high temperature or in combustion experiments to achieve desired phase purity. For example, Stryganyuk et al. (2007), synthesized Ce^{3+} doped $LaPO_4$ nanophosphors by carrying out the solid-state reaction at 1200 ^{o}C in air. Hui et al. (2007), reported a sol-gel combustion method to synthesize LuAG: Ce phosphors under lengthy high temperature treatment (>1400 ^{o}C for 20-30 h). However, the nanoparticles yielded in high temperature processes led to low processability because they did not have any organic groups on the surface and subsequently were not dispersible in water (Wang et al. 2007). And thereby, their applications were very limited.

In recent years, growing attention has been paid to obtain water-soluble lanthanide-doped nanocrystals. Synthesis efforts have been established by using liquid phase synthesis in order to make nanoparticles more preferable for biological applications (Beaurepaire et al. 2004).

Among previous work, oxygen based systems, such as $LaPO_4$, YVO_4 and $Y_2S_iO_5$, were chosen as hosts for some lanthanide ions that emit in visible spectral region because they have high phonon energy (Beaurepaire et al. 2004; Cooke et al. 2006). Later, researchers found that the oxygen based ligands created inhomogeneous boundary surrounding the particle surface, which quenched their fluorescence (Diamente and Veggel 2005). Consequently, researchers started to pursue other materials as substitutes. Fluorides, which have lower phonon energy, became very popular due to their adequate thermal and environmental stability as well as their longer luminescent lifetimes (Stouwdam et al. 2003). Additionally, their very low vibrational energies were established to minimize quenching of the excited state of the rare-earth ions (Wang et al. 2007).

Since lanthanide-based nanocrystals and fluorides are both very promising, several studies of producing water soluble lanthanide-doped LaF_3 nanocrystals have been reported recently. The synthesis of LaF_3 nanocrystals coated by organic compounds containing S and P was first reported by Zhou et al. (2001). Then, Veggel et al. (2002) reported the synthesis of water soluble LaF_3 nanocrystals using citrate or phosphate monoester-base ligands. In their research, ammonium di-n-octadecyldithiophosphate was used as the ligand against particles aggregation. However, the fluorescence was quenched

and the quantum yield was reduced at the same time because the bonded ligands created

inhomogeneous domains near the particle surface and therefore they had poor

dispersibility in solvents. (Stouwdam and Veggel 2002; Wang et al. 2006 Nanotech.;

Wang et al. 2006 J. Mater. Chem.)

Alternatively, hydrothermal synthesis was used to obtain CeF: Tb/LaF (core/shell)

nanoplates (Wang et al. 2006 Chem. Mater.) to investigate their photoluminescence.

Despite the plethora of numerous investigations reported to date, little has been reported

toward synthesizing LaF_3: Ce nanocrystals with good dispersibility in organic solvents

(Riwotzki et al. 2001) with particles synthesized at low temperature. In this thesis, a

simple synthesis route of highly water-soluble LaF_3: Ce nanocrystals is presented. The

proposed synthesis is based on a modified approach to that was developed by Wang et al.

(Wang et al. 2006 Nanotech.; Wang et al. 2006 J. Mater. Chem.), for other lanthanides

such as Eu^{3+}. Water-soluble LaF_3 nanocrystals synthesis was carried out in aqueous

solution at low temperature without using any ligands. These nanocrystals are easily

dispersed in DI-water to form a stable colloidal solution, which provided easier control of

the synthesis.

2.2 Experiments details

To control the concentration of Ce ions, calculations involving determination of proper

quantities of each chemical need to be precisely made. Proportion of La^{3+} ions to Ce^{3+}

ions can be related by the chemical reaction equation below:

$$X\text{LaCl}_3 \cdot 7\text{H}_2\text{O} + Z\text{CeCl}_3 \cdot 7\text{H}_2\text{O} + 3\text{NH}_4\text{F} \longrightarrow \text{La}_x\text{Ce}_z\text{F}_3 + 3\text{NH}_4\text{Cl} + 7\text{H}_2\text{O}$$

Here, X represents the molar percentage of La^{3+} ions, and Z refers to that of Ce^{3+} ions, where $X + Z = 1$. For example, if 5% Ce^{3+} doped LaF_3 nanoparticles are expected to be prepared, $Z = 5\% = 0.05$. Then X would be 0.95. The LaF_3 Nanocrystals doped with Ce at other percentage (1% and 10%) can be calculated by the same means.

2.2.1 Reagents

During this synthesis, all chemicals were used as received without further purification. Ammonium fluoride (NH_4F, 99%), Cerium chlorides hexahydrate ($\text{CeCl}_3 . 7\text{H}_2\text{O}$, 99.99%), and lanthanide chlorides hexahydrate ($\text{LaCl}_3 . 7\text{H}_2\text{O}$, 99.99%) were obtained from Sigma-Aldrich (St Louis, USA). Chitosan was purchased from Sigma-Aldrich (St Louis, USA). And anhydrous methanol was purchase from Alfa Aesar (Ward Hill, USA). LaCl_3 and CeCl_3 were stored in an oven overnight at 75°C to eliminate the possibly absorbed water on the surface prior to synthesis.

2.2.2 Synthesis of LaF_3: Ce nanocrystals

The proposed synthesis of highly water-soluble LaF_3: Ce, follows the approach carried out by Wang et al. (2006 J. Mater. Chem.), reported for other lanthanide: Eu^{3+}. Methanol and DI-water were used as solvents. An experiment was also carried out with DI- water and chitosan (DI-chitosan) in a similar method compared with the previous two. In this research, samples with different levels of Ce (0%, 1%, 3%, 5%, and 10%) were studied

with methanol, and some levels of Ce (0%, 1%, 5%, and 10%) were studied with DI-water and DI-chitosan, respectively.

Summary of the procedures for synthesis are shown as the flow chart in Fig 2.1. More details about the synthesis are given next.
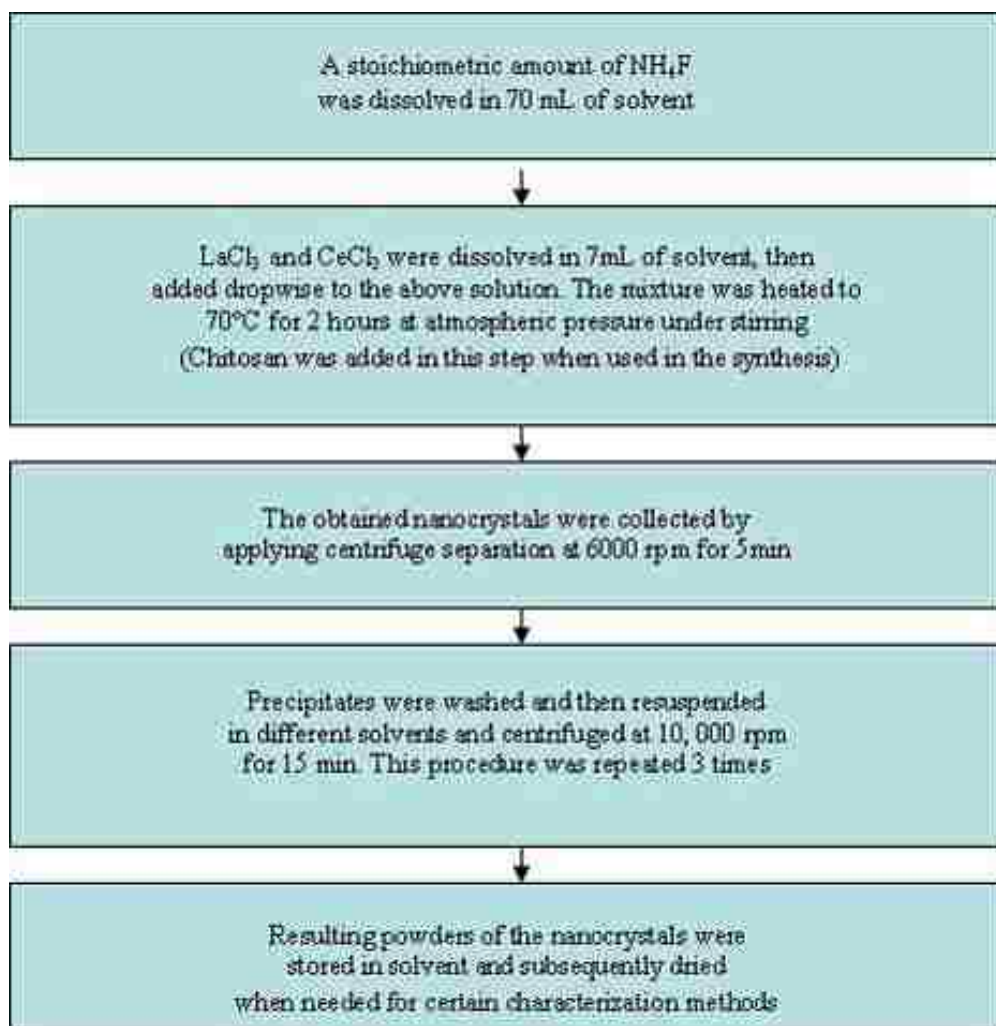
Fig 2.1 Flowchart of synthesis procedures

1) Using methanol as solvent

5% Ce $^{3+}$-doped LaF$_3$ nanocrystals with methanol were prepared as follows: 0. 5670g (15.310 mmol) NH$_4$F was dissolved in 70 mL solvent. 1.8004g (4.850 mmol) LaCl$_3$.7H$_2$O was dissolved in 7mL solvent water (Fig 2.2 left) followed by the addition of 0.0951g (0.255 mmol) CeCl$_3$.7H$_2$O, then instilled drop by drop into the NH$_4$F solution under vacuum (Fig 2.2 right). White precipitates appeared instantly.

Fig 2.2 Dissolve solutions (left) and mix them (right) during the synthesis of LaF$_3$: Ce Nanocrystals

The mixture was heated at 60°C for 15 minutes at atmospheric pressure with continuous stirring at 20 rpm. Evaporation was stopped when the solution decreased to 50 mL in order to avoid solution supersaturation at less volume. Nanocrystals were separated from the colloidal solution using following two methods:

   a)   Method-1: Filtration (Fig 2.3)

Filter papers from Sartorious, Inc., with pore size 0.22 nm were used. The solution

was filtrated immediately by filter funnel, and nanoparticles were collected on filter

paper. Then 20 mL methanol was added to wash nanoparticles again, as was repeated

twice. Powders were collected from the filter paper and subsequently stored overnight

at 75 $^{\circ}$C in the oven.

Fig 2.3 Use of funnels to separate LaF$_3$: Ce nanocrystals from colloidal solution

b) Method-2: Centrifugation (Fig 2.4)

Centrifugation treatment was applied at 6,000 rpm for 5 min then at 10,000 rpm for

10 min. Precipitates were washed and re-suspended in methanol, and then centrifuged

at 10,000 rpm for 15 min. This procedure was repeated 3 times. Resulting powders of

nanocrystals were subsequently dried overnight at 75°C in the oven.

Fig 2.4 Use of centrifuge to separate LaF$_3$: Ce nanocrystals from colloidal solution

0%, 1% and 10% Ce^{3+}-doped LaF$_3$ nanocrystals were prepared by using this method as well; stoichiometryically.

2) Using DI- water as solvent

5% Ce^{3+}-doped LaF$_3$ nanocrystals with DI- water were prepared as follows: 1.8004 g (4.850 mmol) LaCl$_3$.7H$_2$O and 0.0951g (0.255 mmol) CeCl$_3$.7H$_2$O were dissolved completely in 7 mL Distilled- water (DI-water). 0. 5670 g (15.310 mmol) NH$_4$F was dissolved in 70 mL DI- water and mixed with the above solution thoroughly. As a result, white precipitates appeared. Mixture was then consistently heated at 75°C for 2 hours at ambient pressure under stirring. Precipitates were separated by centrifugation at 6,000 rpm for 5 min and then at 10,000 rpm for 10 min. Precipitates were washed with DI-water and applied centrifugation treatment at 10,000 rpm for 15 min; and these procedures were repeated 3 times. The resulting nanocrystals were stored in DI- water in oven at 75°C overnight until completely dry.

The method for preparing 0%, 1% and 10% Ce^{3+}-doped LaF_3 nanocrystals were the same as stated above. Only stoichiometric amount of chemicals need to be adjusted.

3) Using DI- chitosan as deagglomerator

Chitosan is a natural biopolymer and its chemical formula as shown in Fig 2.5.
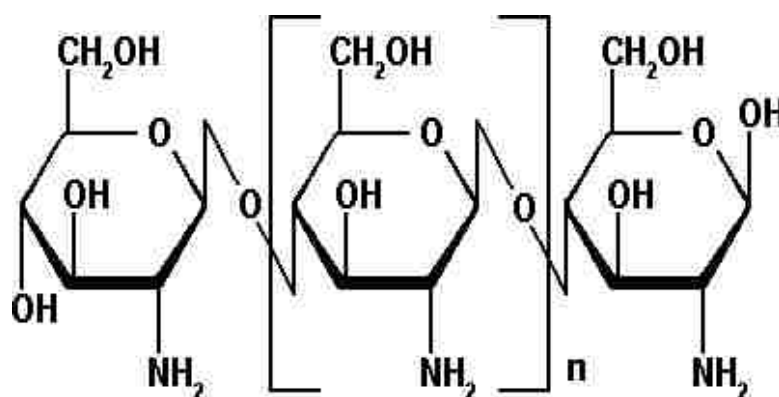
Fig 2.5 Chemical formula of chitosan

Chitosan, a white-colored powder produced by deacetylation of chitin, has a number of applications because it has been shown to be biofunctional and biocompatible (Miyazaki et al. 1981; Kumar 2000). It has been widely used as a plant growth enhancer in agriculture and been adopted to cause the fine sediment particles to bind together as a part of filtration process(Goosen 1996). Moreover, it was allowed to be used as a carrier for drug and gene delivery which could be frequently seen at health stores due to its biocompatible properties (Muzzarelli et al. 1989; Miyazaki et al. 1990; Calvo et al. 1997). Researchers also used it as a bandage and a hemostatic agent to rapidly clot blood. In this work, we used chitosan to prevent nanocrystals from agglomeration and rendered the

nanocrystals water soluble based on similar objective pursued by another research group (Wang et al. 2006 Nanotech.).

5% Ce^{3+}- doped LaF_3 nanocrystals with DI- water were prepared as follows: 0.2 M $LaCl_3$ stock solution was prepared by dissolving $LaCl_3.7H_2O$ in DI- water. 0.2 M $CeCl_3$ stock solution was prepared by dissolving in DI- water as well. Chitosan solution was obtained by dissolving 0.2147 g (1.330 mmol) chitosan in diluted 0.05 M hydrochloric acid. NH_4F solution was obtained by dissolving 0.2222 g (6.000 mmol) NH_4F in 10mL DI- water. Mix 9.5 mL stock $LaCl_3$ solution and 0.5 mL $CeCl_3$ solution thoroughly, then introduce chitosan solution under stirring. After adding NH_4F solution drop wise, white precipitates appeared instantly. Control the pH value of mixture at 6.5 with diluted ammonia solution, then heat the mixture to 75°C for 2 h under stirring.

The resulting products were collected by centrifugation at 6,000 rpm for 5 min, then 10,000 rpm for 10min. Wash precipitates with mixture of DI- water and 0.5% acetic acid and re-suspend in DI- water, and then centrifug at 10,000rpm for 15 min. These procedures were repeated 3 times. Resulting powders of the nanocrystals were stored in DI- water and subsequently dried at 75°C in the oven at ambient temperature.

The same method has been applied for preparing 0%, 1% and 10% Ce^{3+} -doped with LaF_3 nanocrystals.

Chapter 3

Microstructural Characterization

Microstructural characterization methods include X-ray diffraction (XRD), scanning electronic microscopy (SEM) and transmission electron microscopy (TEM). The phase structures of nanoparticles were characterized by XRD. The morphologies of the nanoparticles were investigated by SEM and TEM. The particles size distribution (PSD) was carried out by an imaging software (Image J, NIH, USA) coupled with the TEM micrographs.

3.1 X-ray Diffraction

X-ray diffraction (XRD) is one of the most important characterization tools to determine crystal structure and lattice parameters of any crystalline compound (Warren 1990). Each crystalline solid can be presented as an infinite regular three-dimensional distribution of atoms in space. They form a series of parallel planes separated from one

another by a distance d, which exists in a number of different orientations (Zhou et al. 2001). In XRD, as a beam, which is based on constructive interference of monochromatic X-rays and a crystalline sample, travels through any substance, the resulting diffracted beams are detected and the intensity decreases with the distance traveled through the substance. If the sample is crystalline, the interaction of the incident rays will produce constructive interference (and a diffracted ray). Meanwhile, detected intensities of diffracted beams will vary in different directions. According to Bragg's Law ($n\lambda = 2d \sin \theta$), which relates the wavelength of electromagnetic radiation (λ) to the diffraction angle (θ) and the lattice spacing in a crystalline sample (d), a unique diffraction pattern is produced, characteristic of the crystal structure of the sample .

In this thesis, the X-ray diffraction was carried out using a Phillips powder 2θ X-ray diffractometer. This is to investigate the elemental compositions of the synthesized samples carried out in the three different solvents.

3.1.1 XRD for samples prepared using methanol

Fig 3.1 XRD patterns of the LaF₃: Ce nanocrystals with different Ce concentrations (0%, 3%, 5%, 8% and 10%) with using methanol as solvent

XRD patterns of the LaF$_3$:Ce^{3+} nanocrystals with 0%, 3%, 5%, 8% and 10% Ce concentrations are shown in Fig 3.1. The phase evolution shown by XRD indicates that LaF$_3$ appears to crystallize directly from 0% doping to 10% doping, and these samples are crystallized well: the peak intensities and positions of these nanocrystals are similar and agree well with the data in the Powder Diffraction File (PDF) standard card. It can also been found that when the Ce^{3+} ions are doped in the LaF$_3$ host, no difference is observed between the diffraction patterns of LaF$_3$: Ce^{3+} and LaF$_3$.

3.1.2 XRD for samples prepared using DI- water
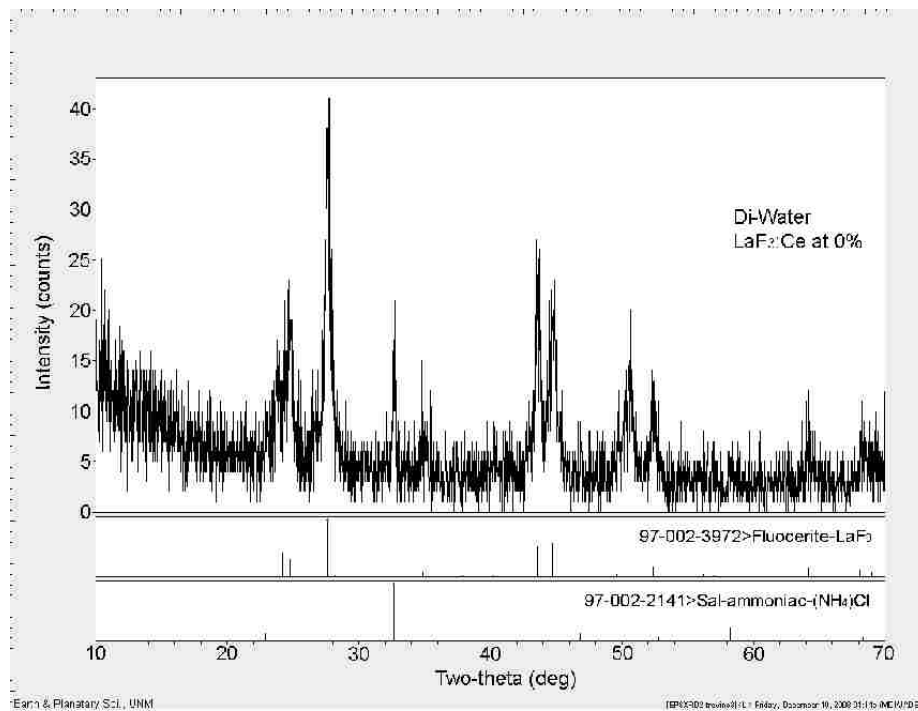
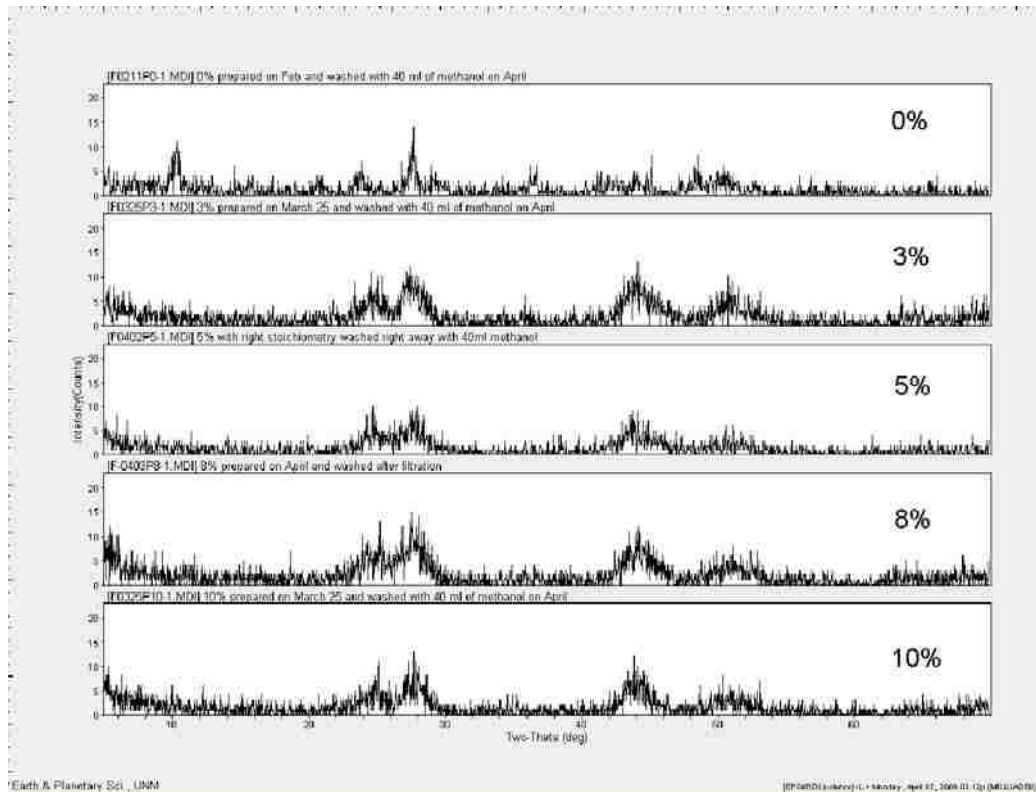**Fig 3.2** XRD pattern of the LaF_3: Ce at 0% with using DI- water as solvent.

Fig 3.3 XRD patterns of the LaF_3: Ce nanocrystals with different Ce concentrations (1%, 3%, 5%, and 10%) with using DI- water as solvent.

The XRD patterns of the LaF$_3$: Ce nanocrystals with using DI- water are given in Figs 3.2 and 3.3. The diffraction patterns also agree well with the pure hexagonal LaF$_3$ and CeF$_3$ crystals in PDF. The results show that the structure and size of nanocrystals do not change when more Ce ions are doped. Compared with Fig 3.1, the diffraction peaks in Fig 3.2 and Fig 3.3 are sharper, clearly revealing that the particles made with Di- water are larger than those made with methanol.

### 3.1.3 XRD for samples prepared using DI- chitosan

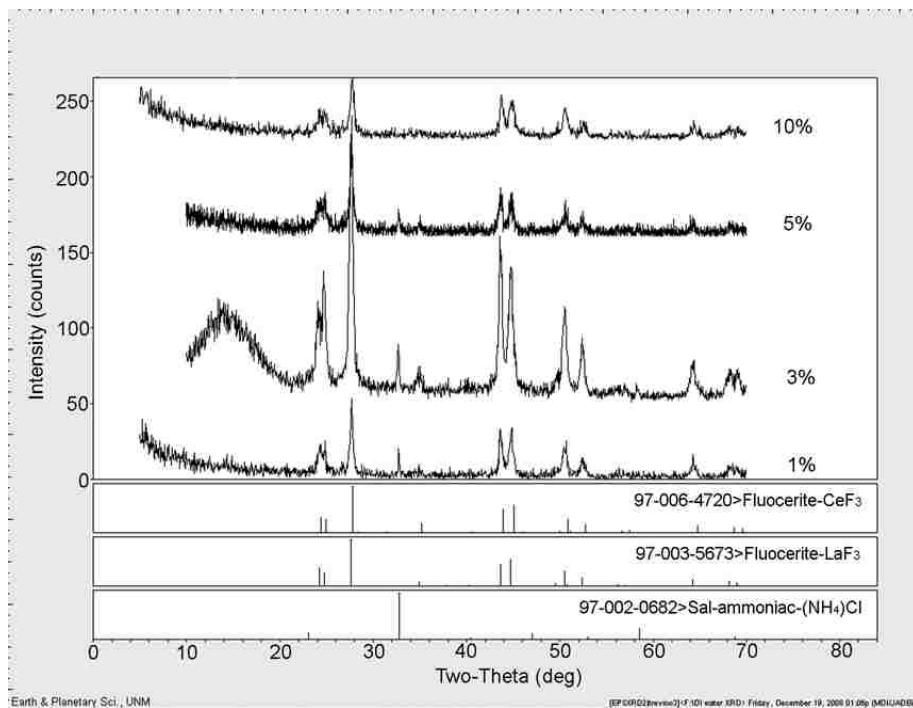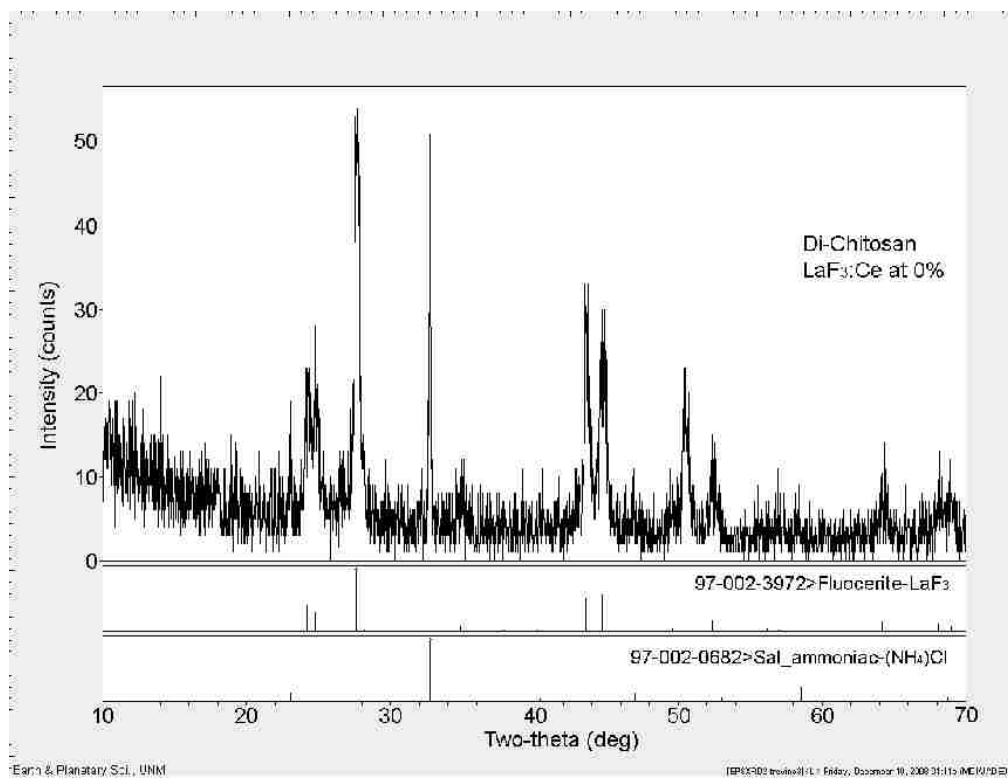**Fig 3.4** XRD pattern of the LaF$_3$: Ce at 0% with using DI- chitosan as solvent.

28
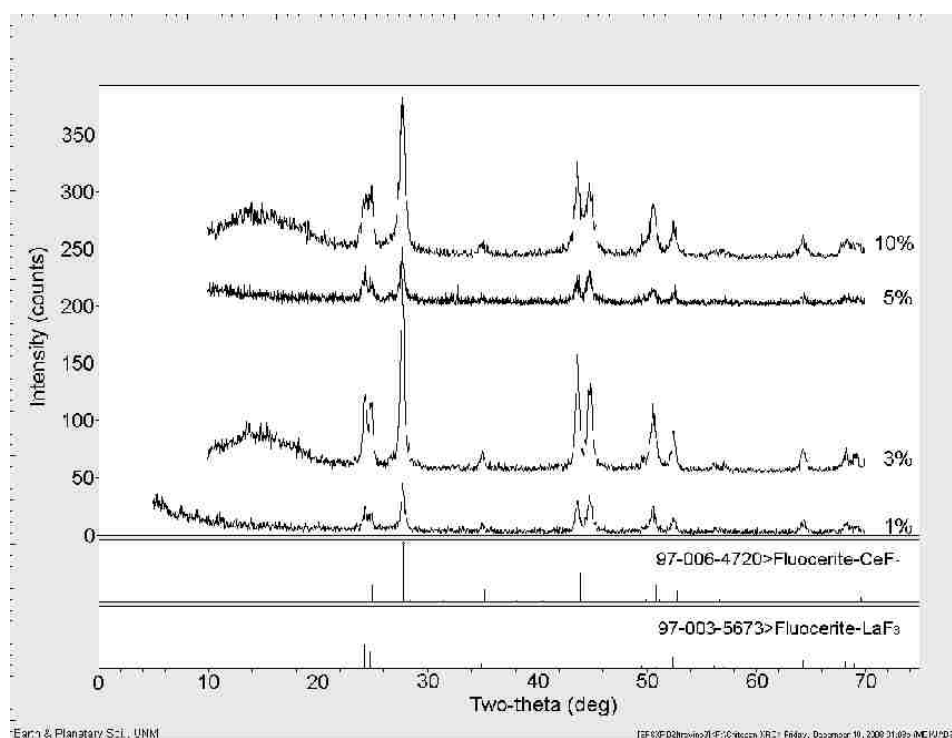
Fig 3.5 XRD patterns of the LaF$_3$: Ce nanocrystals with different Ce concentrations (1%, 3%, 5%, and 10%) with using DI- chitosan as solvent.

In Figs 3.4 and 3.5, analysis of the powder diffraction patterns shows that the spectrum peak positions and intensities agree well to the literature data of the bulk LaF$_3$ and CeF$_3$, suggesting that the compounds are free of impurity phases. That is to say, NH$_4$Cl ions have been successfully washed off by solvents during synthesis. The identical shape and intensity of diffraction peaks of NCs with using DI- chitosan as those with using DI-water show that the particle sizes are very close (Zhang and Lu 2007). And both of them offer larger particles size than those with using methanol.

XRD patterns can be also used to estimate nanoparticles average sizes according to the Debye-Scherrer equation, D= 0.90 λ/ βcos θ (Wang et al. 2006 J. Mater. Chem.; Stryganyuk et al. 2007; Zhang and Lu 2007). In this equation, D is the average grain size,

29

λ refers to the x-ray wavelength, and β and θ are full width at half maximum (FWHM) of an observed peak and the observed peak angle, respectively (Wang et al. 2007). Here, 2θ, where strongest peak appears, is used to calculate the average size of NCs. From Figs 3.1 to 3.5, it can be seen that 2θ appears around 28° for all cases. And NCs with methanol have broader bandwidths than those with DI- water and DI- chitosan, meaning β of methonal is smaller than that of DI- water and with DI- chitosan. By using Scherrer equation, we can estimate that the NCs with DI- water and DI- chitosan have larger particle sizes than those with methanol (Wang et al. 2007).

3.2 Scanning electron microscopy

In typical scanning electron microscopy (SEM), the electrons are transmitted from an electron gun trigger the sample surface to produce signal. Then the signals collect information about the surface composition, morphology and other properties and transmit them to receiver. In our research, the SEM measurements were carried out on a Hitachi S-5200 nano scanning electron microscope, exhibiting the surface morphology of nanoparticles.

% Ce	Filtration By Funnel	Filtration By Centrifuge
3%		
8%		
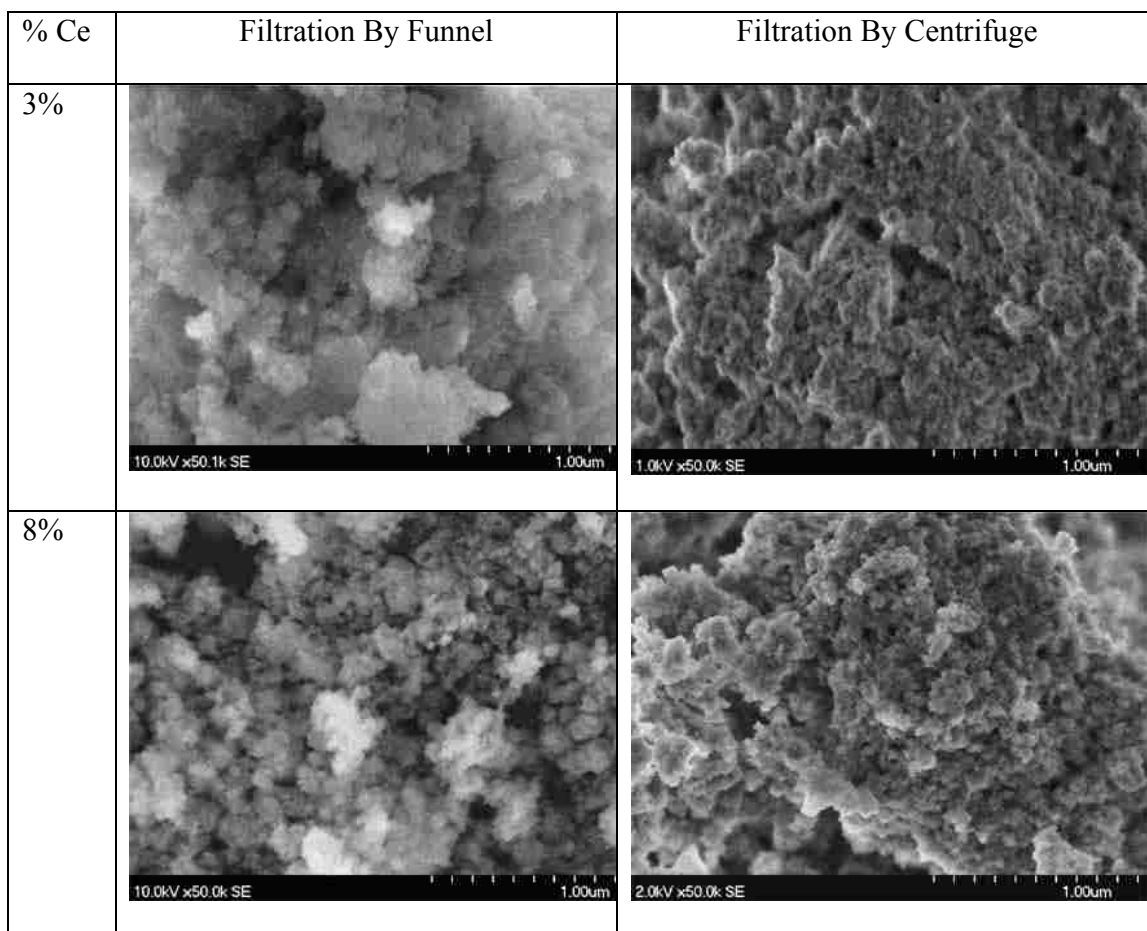
Fig 3.6 SEM images of the LaF_3: Ce nanocrystals with methanol obtained by a funnel and by a centrifuge, respectively.

According to SEM images of nanoparticles with methanol shown in Fig 3.6, it can be seen that synthesized powder by using a funnel (left) was severely agglomerated, while the particles by using a centrifuge (right) offered less agglomeration. Thus, using a centrifuge to separate nanoparticles from collide solution instead of a funnel could offer better results. Therefore, a centrifuge was utilized in the next synthesis in this research.

3.2.1 SEM microscopy of samples prepared using methanol

Through SEM analysis, we were able to identify particles with methanol of irregular shapes between 3 nm and 10 nm with an average size of close to 7 nm. And the particles were observed to form agglomerates. Figs 3.7 through 3.10 show SEM results of LaF_3: Ce particles generated at various concentrations of NCs with methanol.
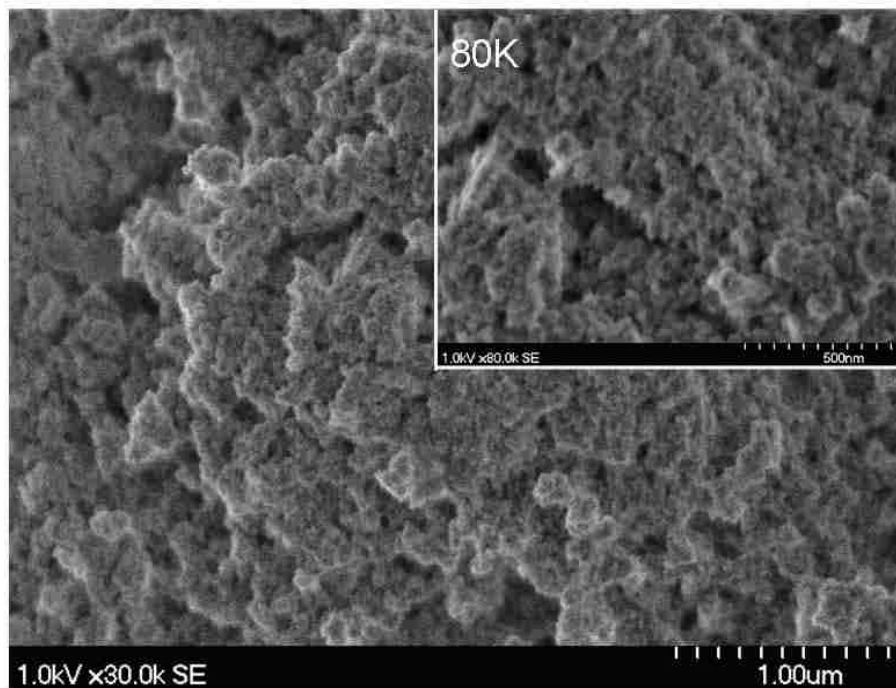

Fig 3.7 SEM images of the LaF_3: Ce at 3% nanocrystals with methanol
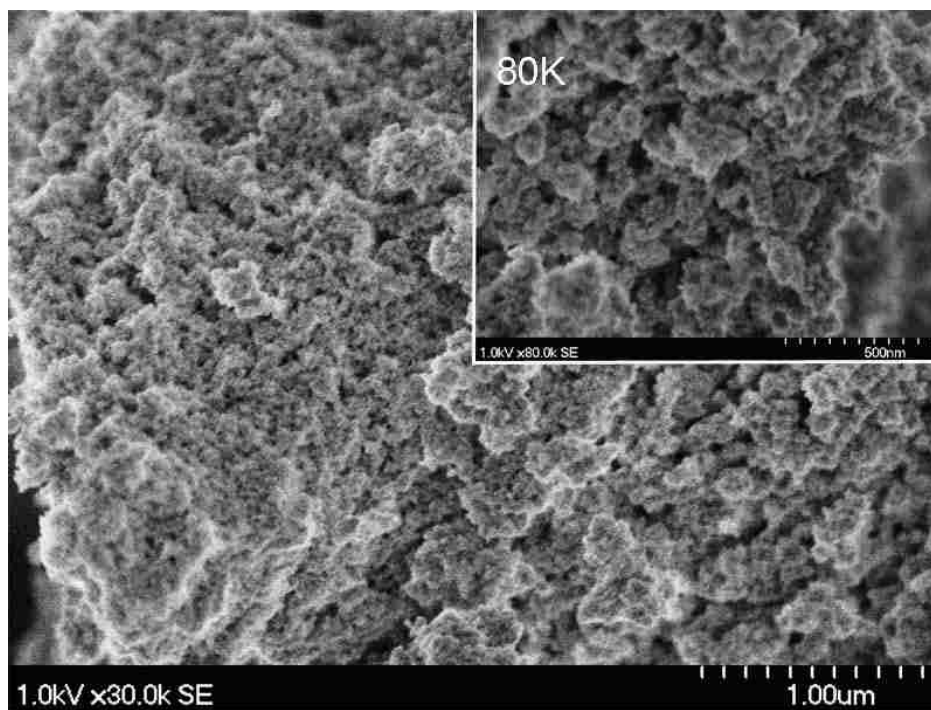
Fig 3.8 SEM images of the LaF$_3$: Ce at 5% nanocrystals with methanol
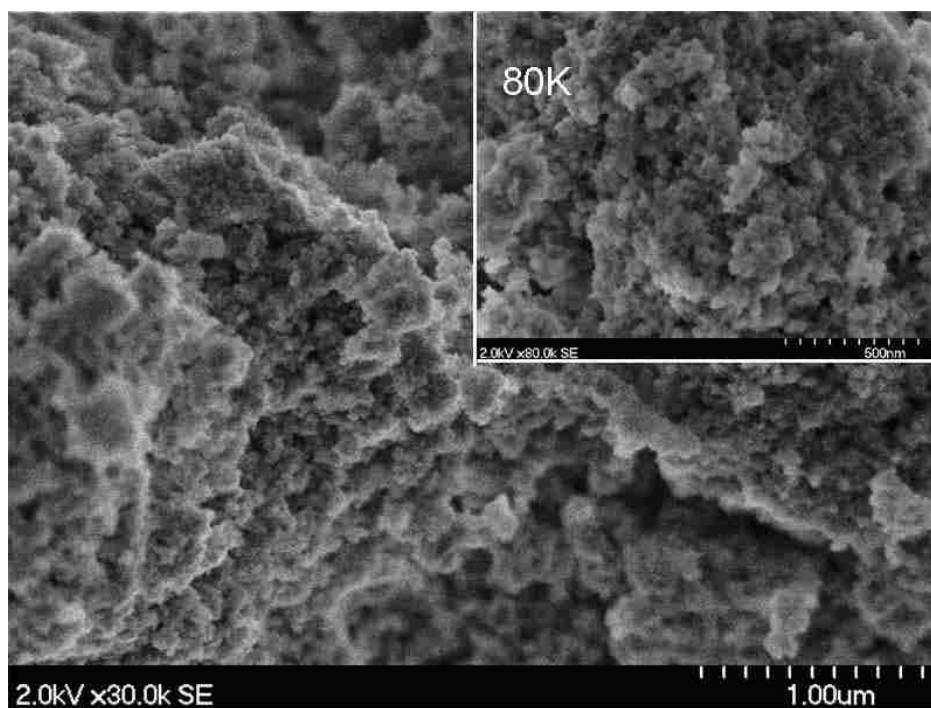
Fig 3.9 SEM images of the LaF$_3$: Ce at 8% nanocrystals with methanol
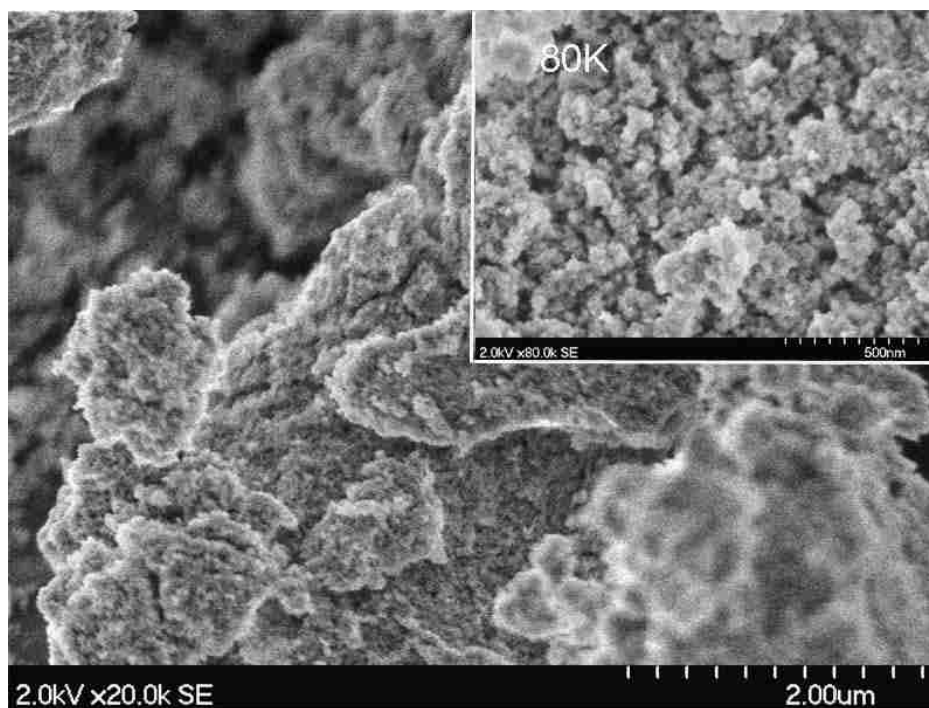
Fig 3.10 SEM images of the LaF$_3$: Ce at 10% nanocrystals with methanol

3.2.2 SEM microscopy for samples prepared using DI- water

Figs 3.11 -3.14 are SEM micrographs of LaF$_3$: Ce particles generated at various

concentrations with DI- water. From the low magnification SEM images, one can see that

the products are composed of nanoscale particles, and they have well-defined shapes

compared to NCs with methanol. The high magnification SEM images indicate that the

nanoparticles average size is about 20nm and approximately spherical in shape.

34
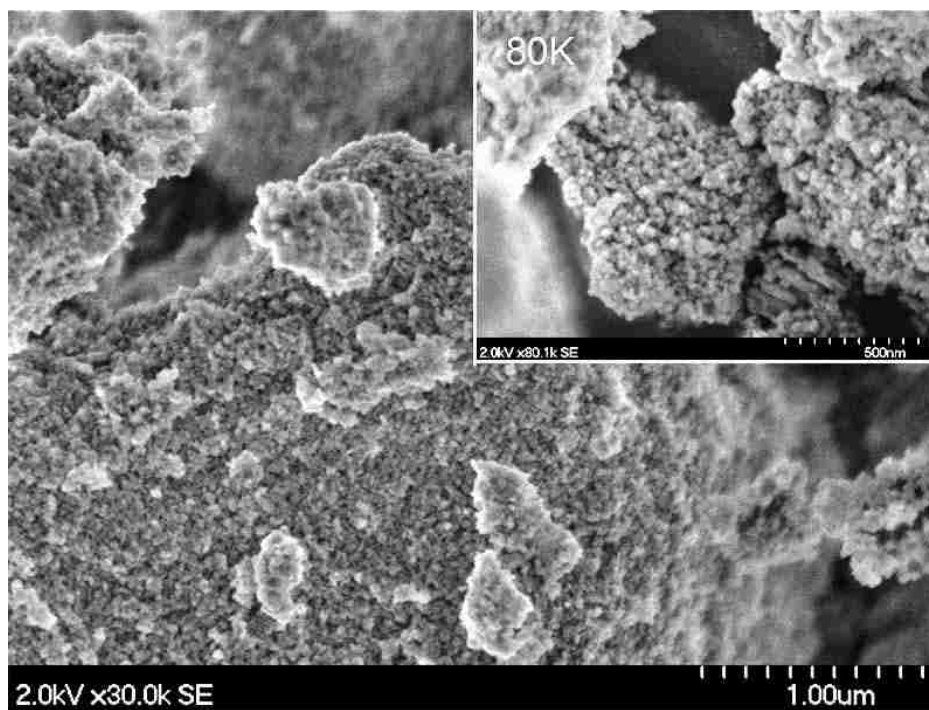
Fig 3.11 SEM images of the LaF$_3$: Ce at 1% nanocrystals with DI- water

Fig 3.12 SEM images of the LaF$_3$: Ce at 3% nanocrystals with DI- water

Fig 3.13 SEM images of the LaF$_3$: Ce at 5% nanocrystals with DI- water
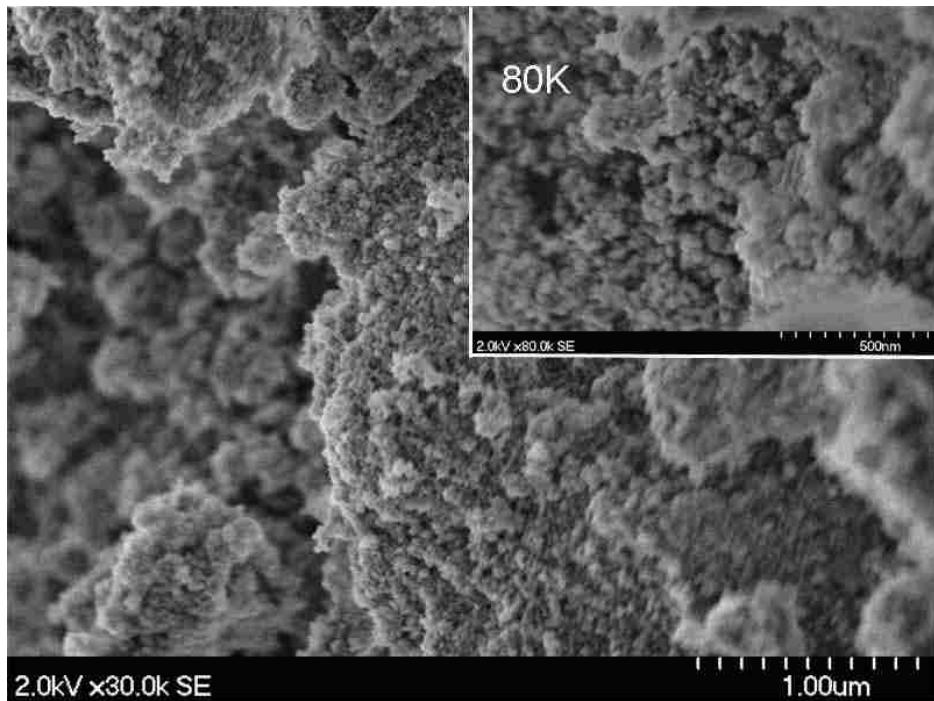
Fig 3.14 SEM images of the LaF$_3$: Ce at 10% nanocrystals with DI- water

36

3.2.3 SEM microscopy for sample prepared using DI- chitosan

From Figs 3.15 to 3.18, one can observe SEM micrographs of LaF$_3$: Ce particles doped at various with DI- chitosan. The low magnification images show the general view of nanoparticles and the high yield of nanoparticles can be synthesized by this means. And the high magnification images indicate that the particles are with a mean diameter of 20 nm and spherical in shape as well.
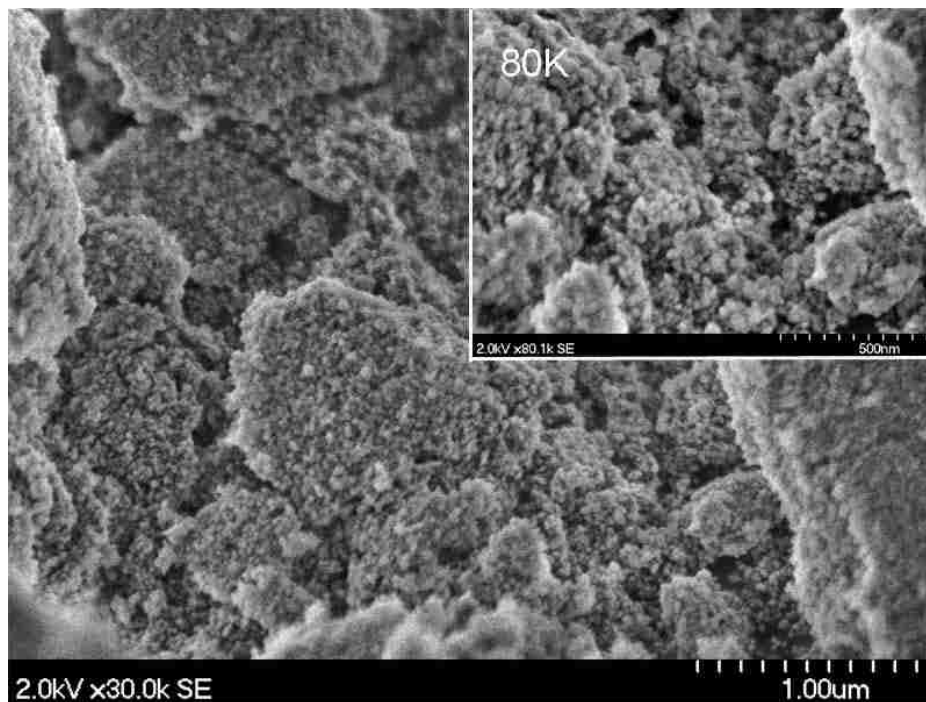
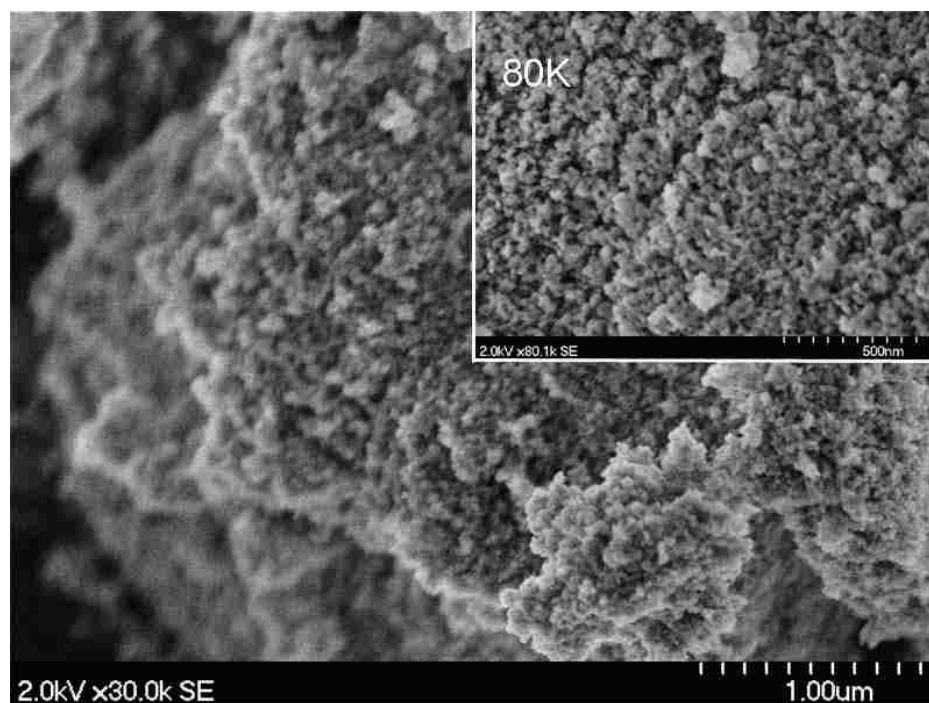**Fig 3.15** SEM images of the LaF$_3$: Ce at 1% nanocrystals with DI- chitosan

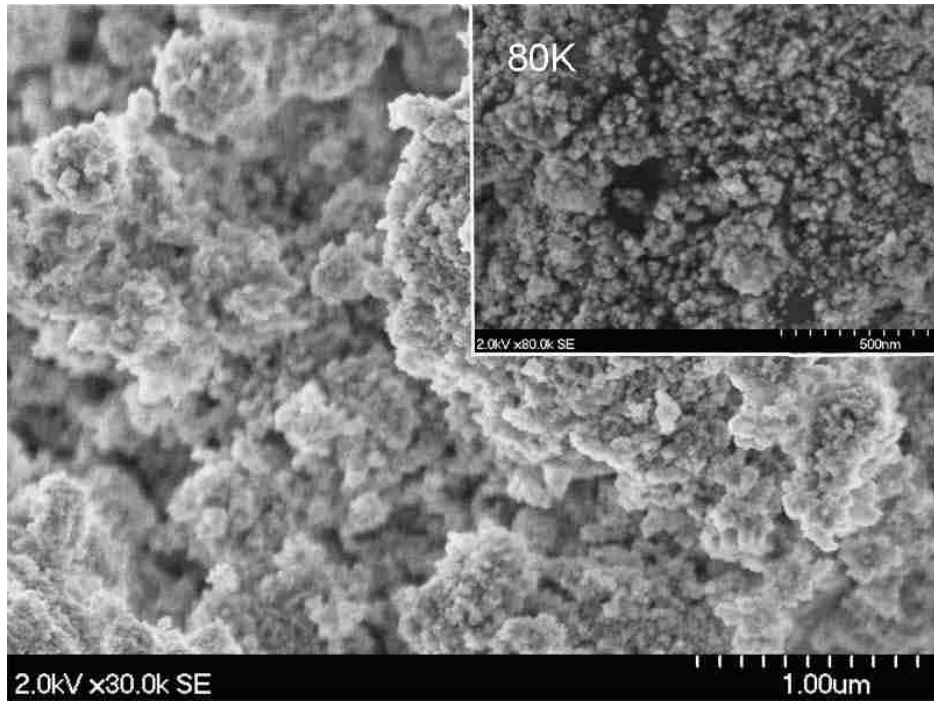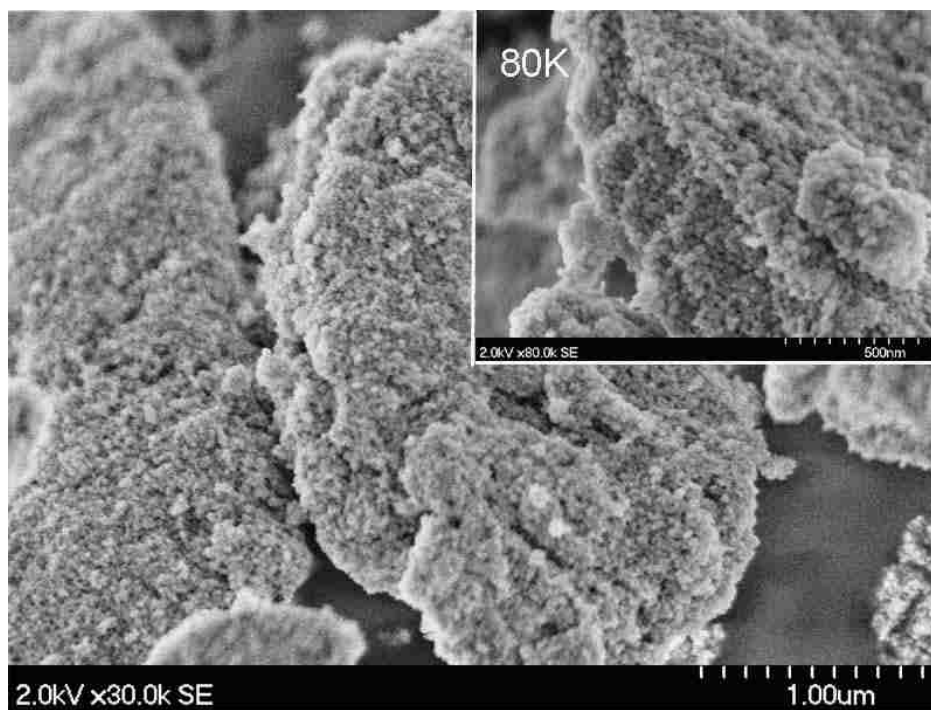**Fig 3.16** SEM images of the LaF$_3$: Ce at 3% nanocrystals with DI- chitosan
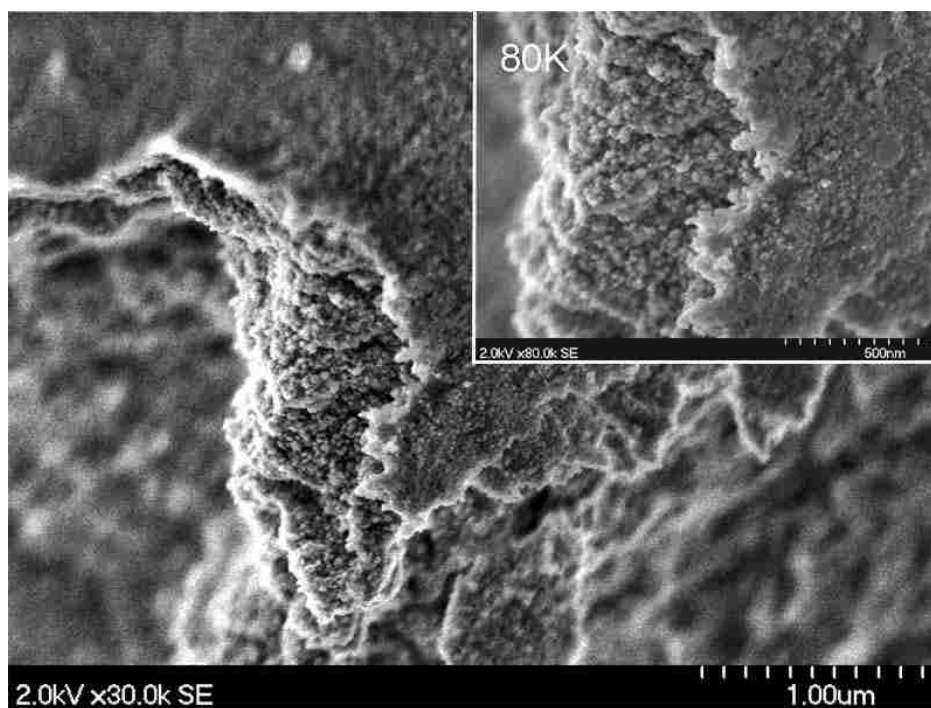
Fig 3.17 SEM images of the LaF$_3$: Ce at 5% nanocrystals with DI- chitosan
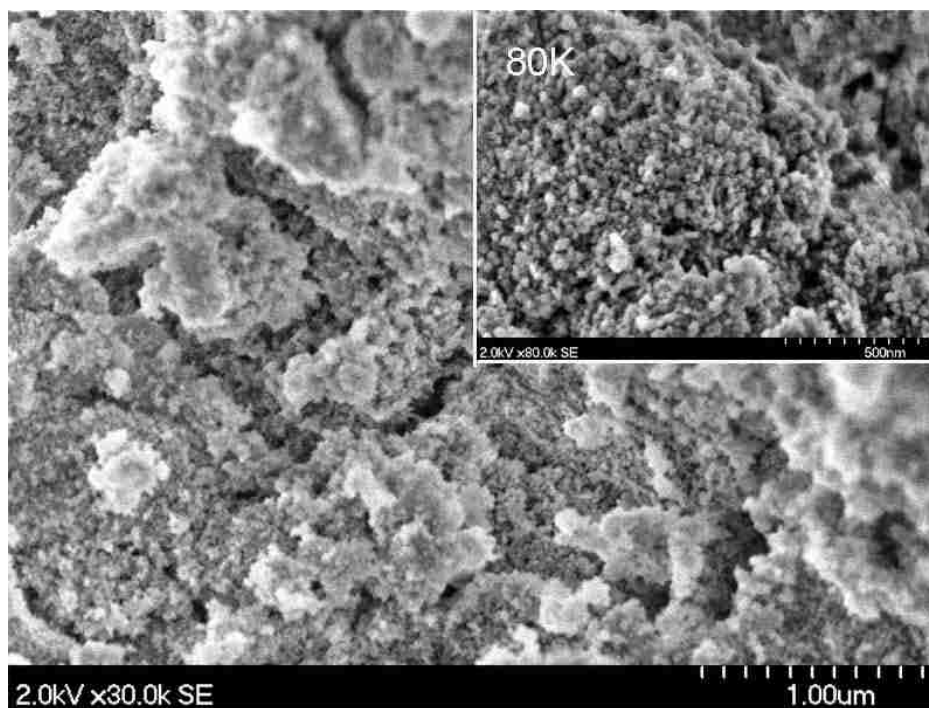
Fig 3.18 SEM images of the LaF$_3$: Ce at 10% nanocrystals with DI- chitosan

3.3 Transmission Electron Microscopy

The Transmission Electron Microscope (TEM, JOEL 2010) images of the NCs were acquired to investigate the structures, shapes as well as sizes of the nanoparticles. Images providing further insight into the nanometer-scale details of particles can be obtained. For our research, the TEM was operated at an acceleration voltage of 200 KV. Samples were prepared by diluting the solution to 0.1 g/L and sonicated sufficiently. Then a couple of drops of the diluted particle dispersion were put on a thick carbon-coated copper grid with excess solutions immediately removed. It was allowed to dry completely before the samples were placed in the TEM grids.

In Fig 3.19 and Fig 3.30 one can observe that nanoparticles are in the forms of spherical and hexagonal shapes and are well dispersed when generated from DI- water and DI- chitosan synthetic routes independent of the Ce dopant amount. The powders synthesized in DI- water and DI- chitosan are less agglomerated than those obtained with methanol (see Figs 3.19 and 3.20). It can also be seen that the average particle size is in the range from 15 nm to 20 nm for both DI- water and DI- chitosan suspensions. Methanol based suspension exhibits an average size of about 7 nm with apparent agglomeration. This result agrees well with the XRD analysis regarding the particle size.

3.3.1 TEM results of using methanol
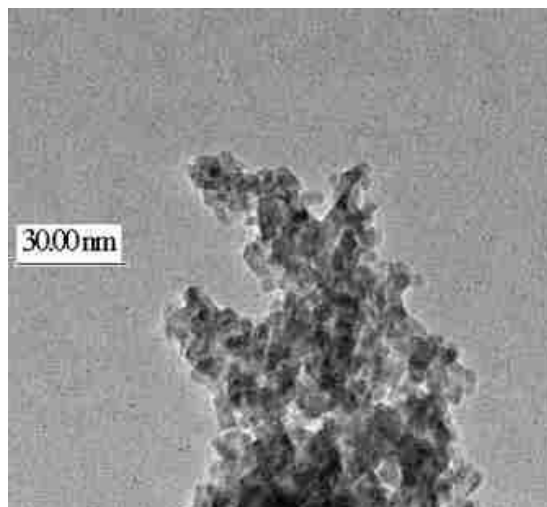
Fig 3.19 TEM images of the 3% doped- Ce^{3+} LaF_3 nanocrystals with methanol
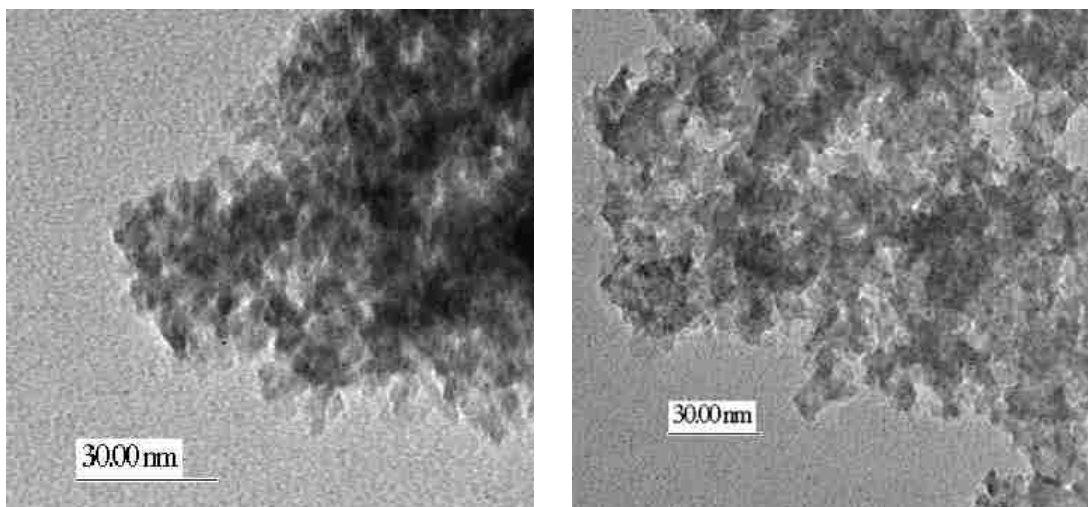
Fig 3.20 TEM images of LaF$_3$: Ce at 5% (left) and at 10% (right) nanocrystals with methanol.

3.3.2 TEM results of using DI- water
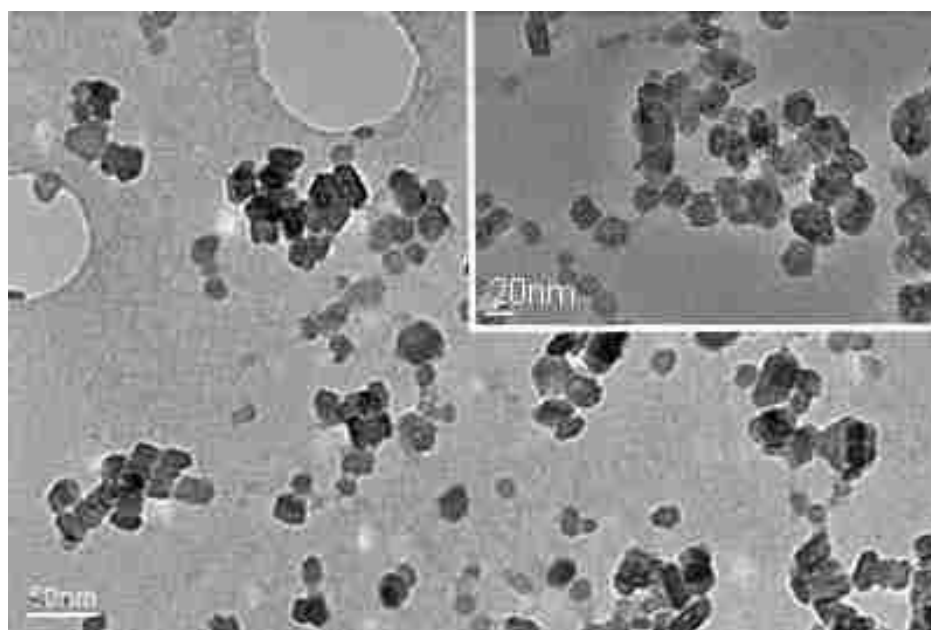
Fig 3.21 TEM images of LaF$_3$: Ce at 0% nanocrystals with DI- water.
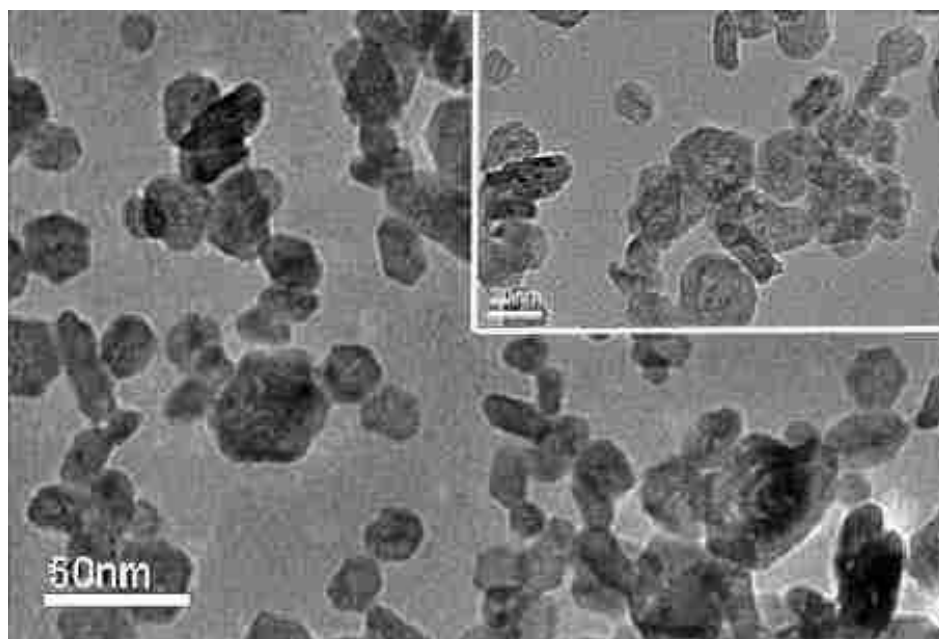
Fig 3.22 TEM images of LaF$_3$: Ce at 1% nanocrystals with DI- water.
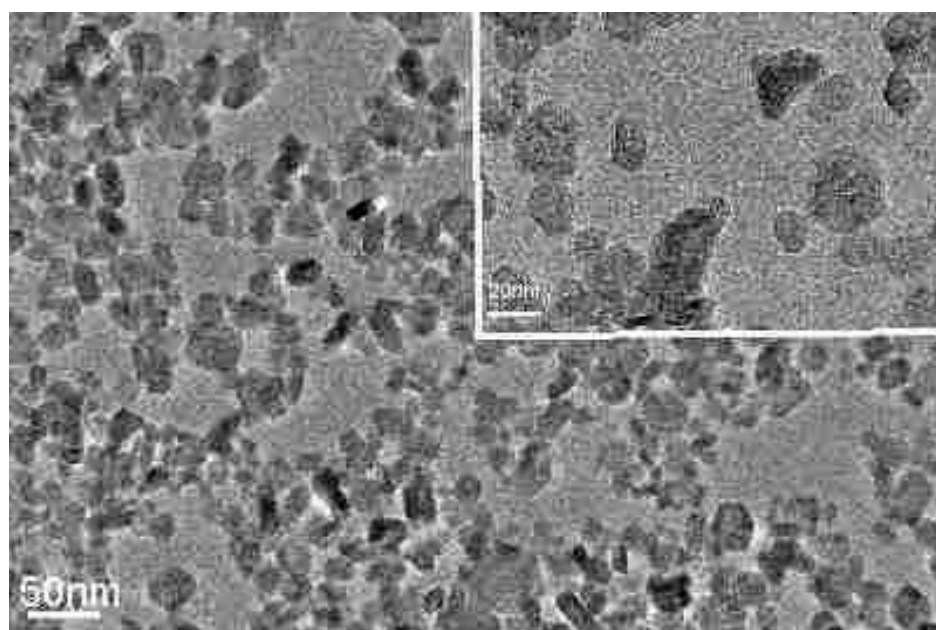
Fig 3.23 TEM images of LaF$_3$: Ce at 3% nanocrystals with DI- water.
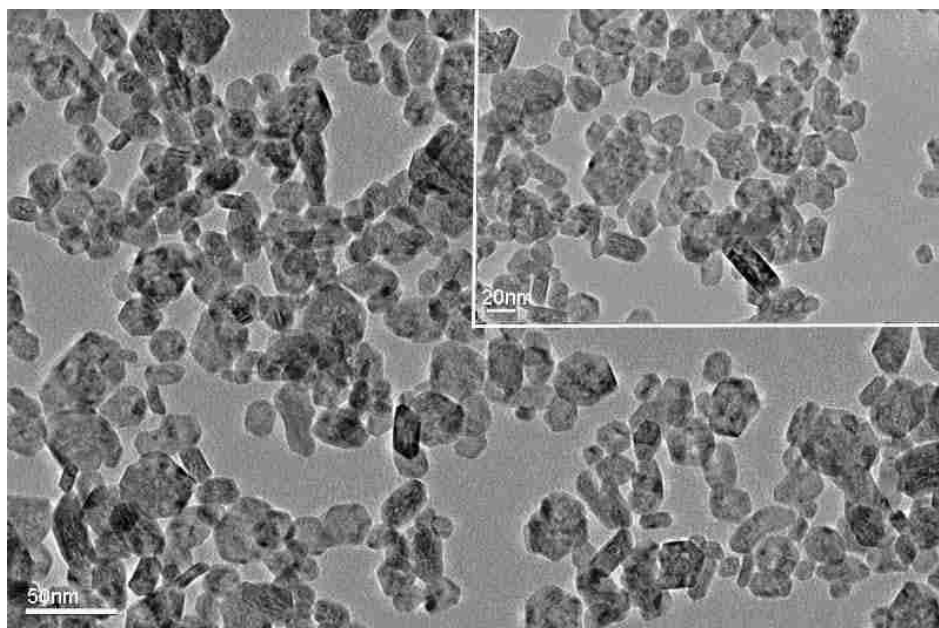
Fig 3.24 TEM images of LaF$_3$: Ce at 5% nanocrystals with DI- water.
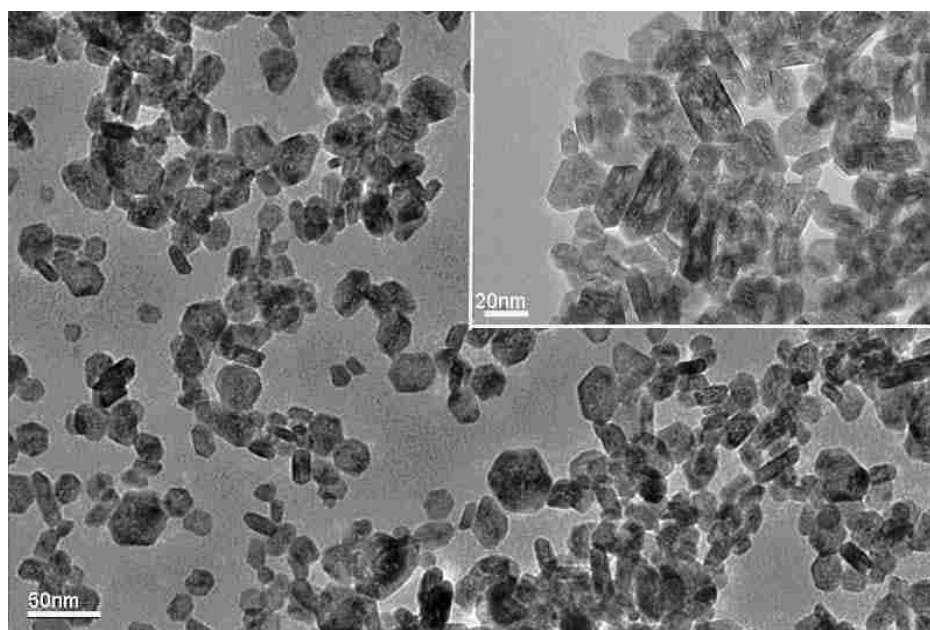
Fig 3.25 TEM images of LaF$_3$: Ce at 10 % nanocrystals with DI- water.

3.3.3 TEM results of using DI-chitosan
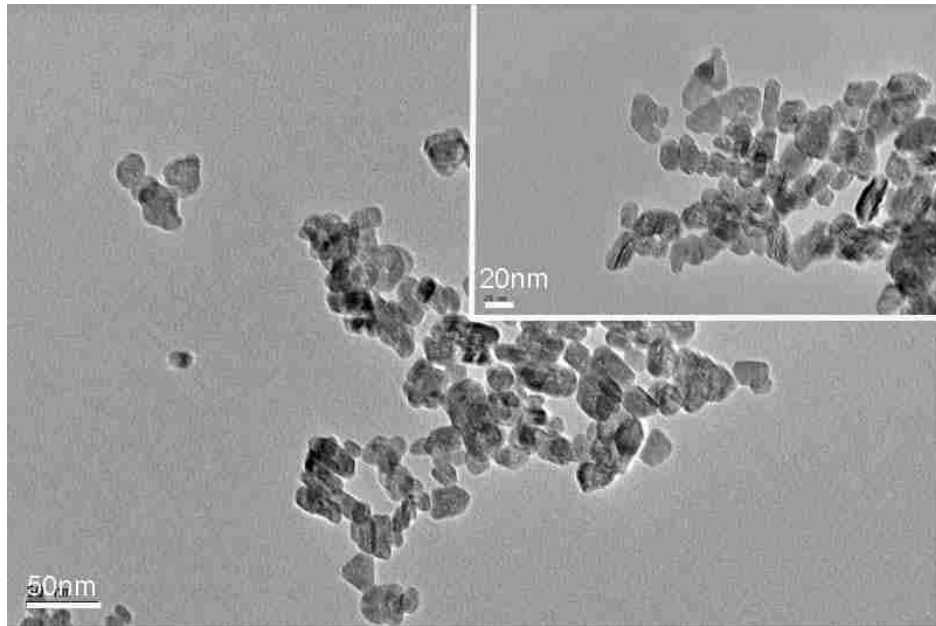
Fig 3.26 TEM images of LaF$_3$: Ce at 0 % nanocrystals with DI- chitosan
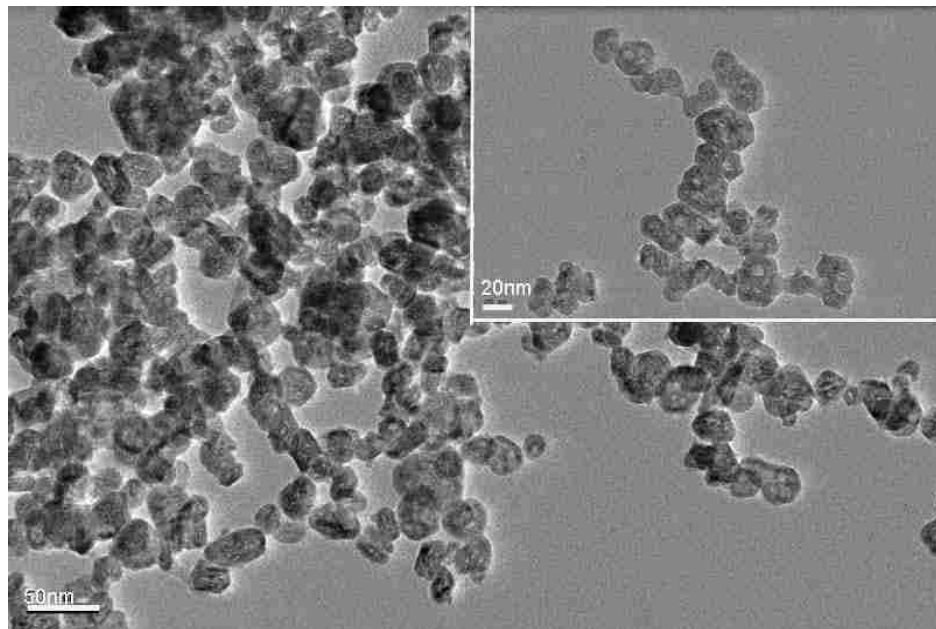
Fig 3.27 TEM images of LaF$_3$: Ce at 1 % nanocrystals with DI- chitosan
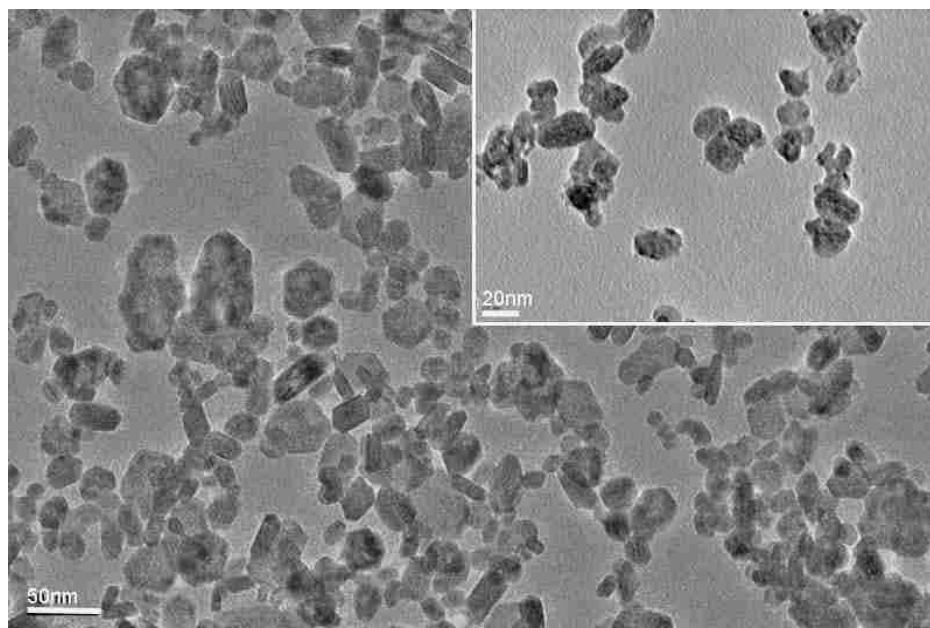
Fig 3.28 TEM images of LaF$_3$: Ce at 3 % nanocrystals with DI- chitosan
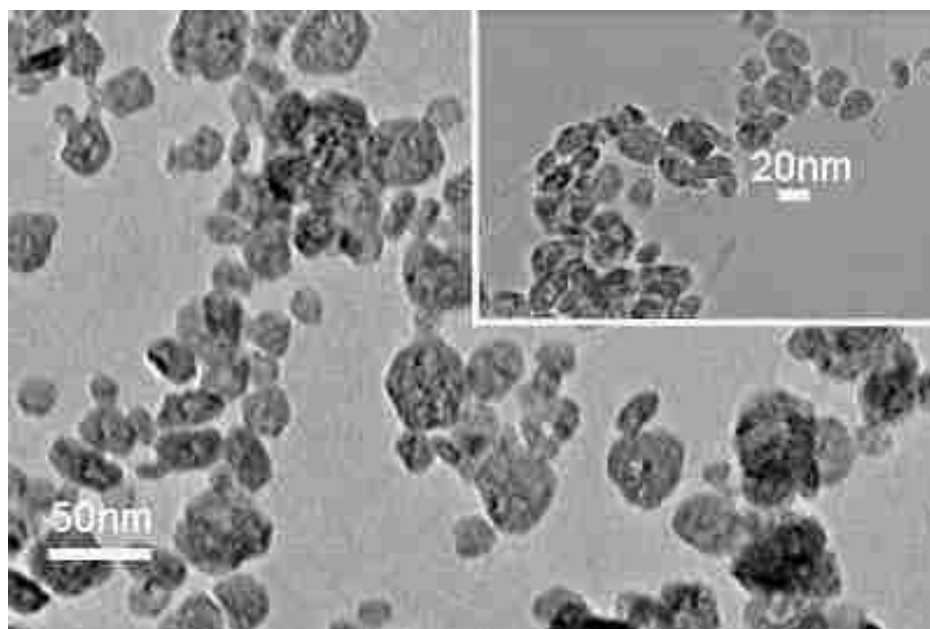
Fig 3.29 TEM images of LaF$_3$: Ce at 5 % nanocrystals with DI- chitosan.
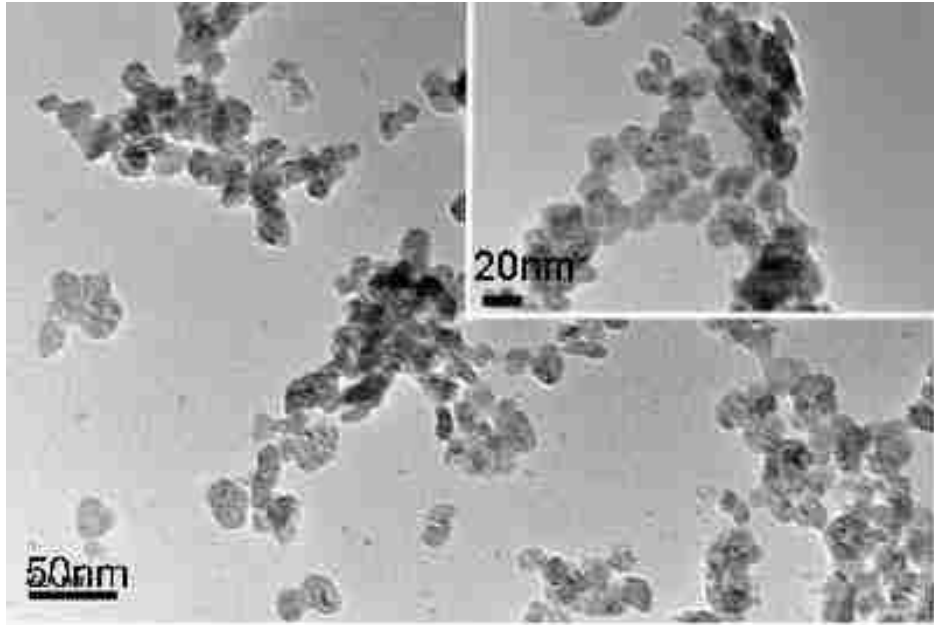
Fig 3.30 TEM images of LaF$_3$: Ce at 10 % nanocrystals with DI- chitosan
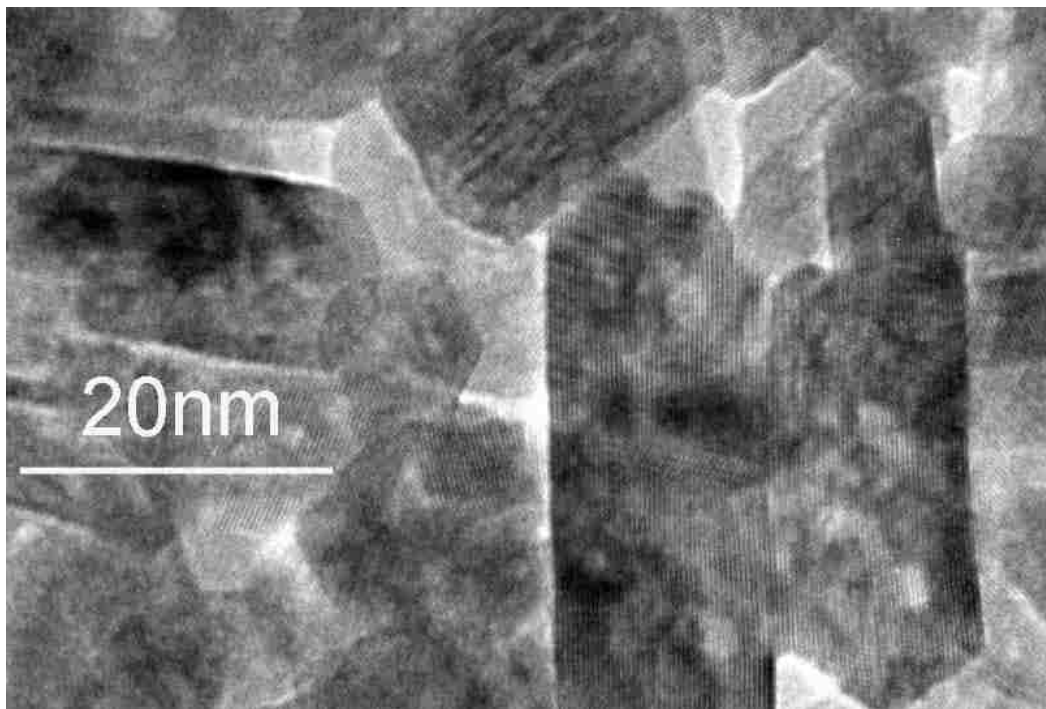
Fig 3.31 TEM images of LaF$_3$: Ce at 10 % nanocrystals with DI- water
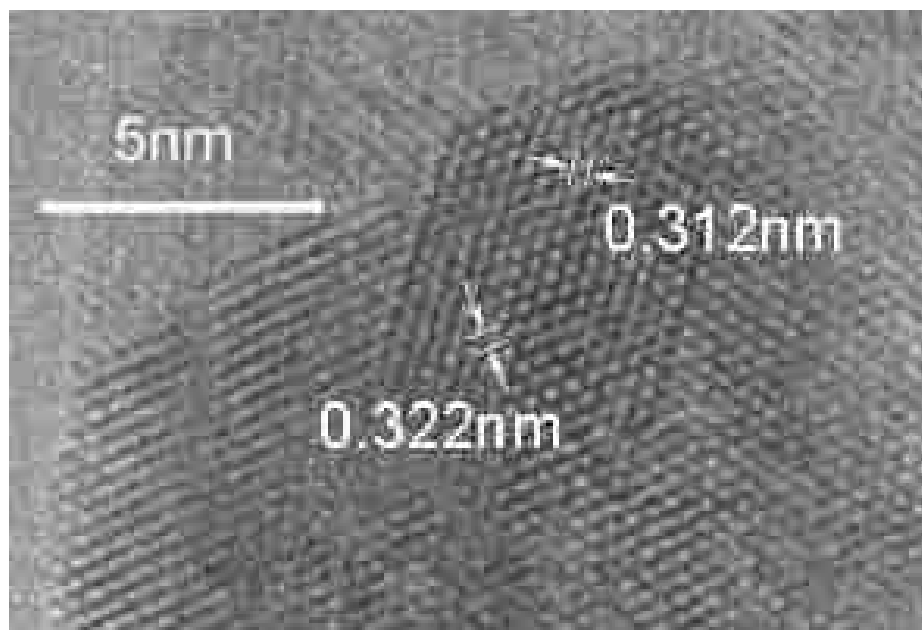
Fig 3.32 TEM images of LaF$_3$: Ce at 10 % nanocrystals with DI- chitosan

From Figs 3.31 and 3.32, one can observe that in higher magnifications nanoparticles display lattice fringes, indicating that they have high crystallinity. In Fig 3.32, nanocrystals which are crystallized with the interplanar spacing of 0.322nm correspond to the (111) crystal plane of LaF$_3$ in PDF standard card. And nanocrystals with interplanar spacing of 0.312nm correspond to the (102) crystal plane of CeF$_3$. The consistent crystal lattice planes seen on nanocrystals prove that the elongated particles are not composed of agglomerated smaller particles. Instead, they are well-dispersed from each other (Veggel 2002).

3.4 Particle Size Distribution (PSD) Analysis

An image analysis software (Image J®) is used to analyze particle sizes from the TEM images of the LaF_3: Ce^{3+} nanoparticles with DI- chitosan and DI- water. Because the samples with methanol only generate agglomerates, PSD analysis is not carried out. In the rest of the thesis, we will focus the fluorescence performance testing on fluorophores dispersed in DI- water only.

A count of 400 particles is used in each case for the particle distribution analysis. They are collected from several images. Only particles with clear shape and boundary are chosen and measured. Figs 3.33 through Fig 3.42 show the size distribution results of particles from various conditions of synthesis using the student's T-test approach. It was calculated that the particles with DI- chitosan have a mean diameter of 17.59 nm and a broad size distribution from 7 nm to 43 nm. Whereas the particles generated by using DI-water are found to have an average size of 19.87 nm which is larger than DI- chitosan. And the fact that nanoparticles with methanol have smaller average particle size than those with DI- water and with DI- chitosan, respectively, agrees well with the estimation of particle size from XRD patterns.

3.4.1 PSD of sample prepared using DI- water
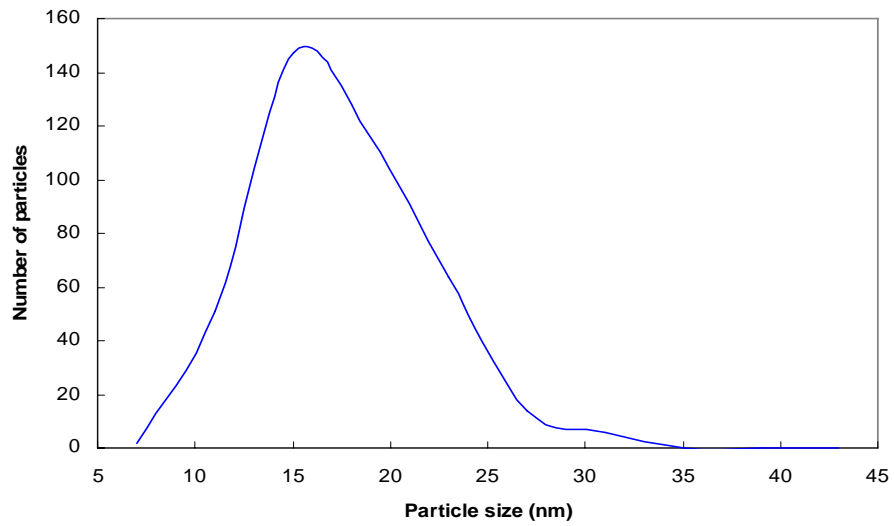
Fig 3.33 particle size distribution of LaF$_3$: Ce at 0% nanocrystals with DI- water
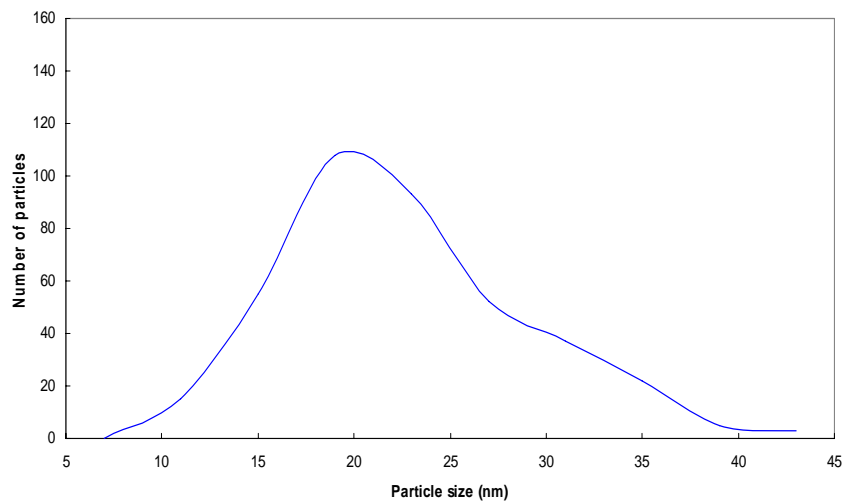
Fig 3.34 particle size distribution of LaF$_3$: Ce at 1% nanocrystals with DI- water
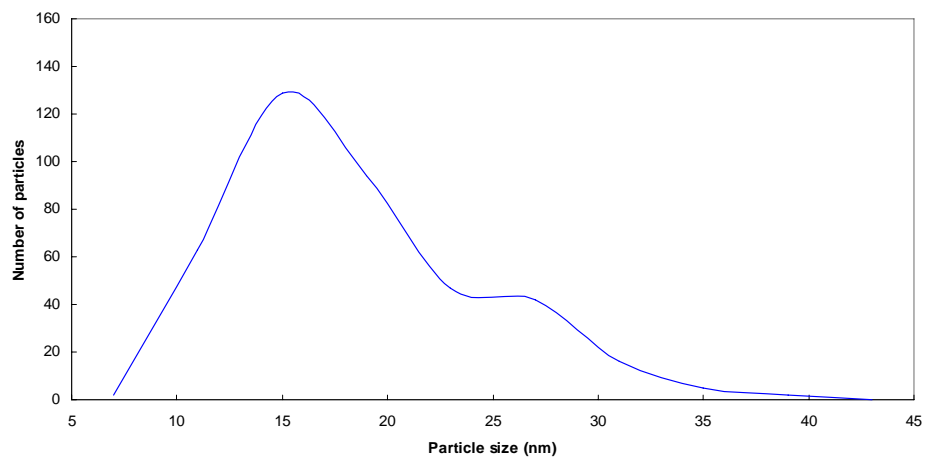
Fig 3.35 particle size distribution of LaF$_3$: Ce at 3% nanocrystals with DI- water
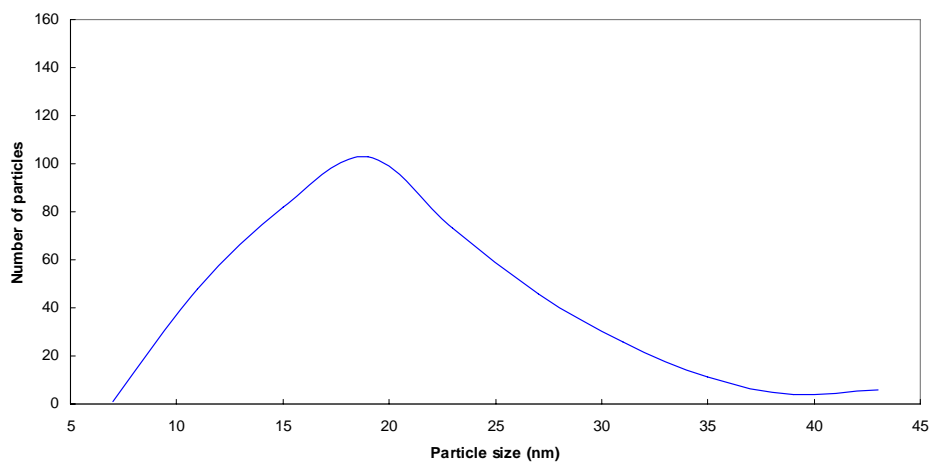
Fig 3.36 particle size distribution of LaF$_3$: Ce at 5% nanocrystals with DI- water
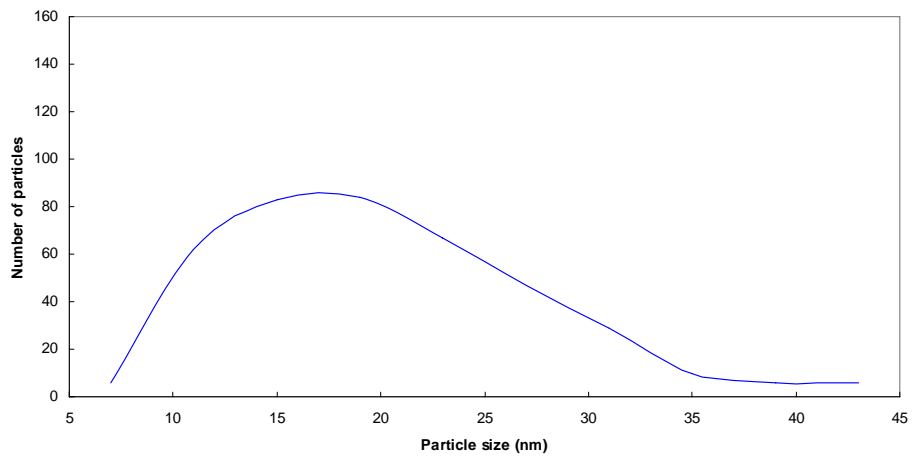
Fig 3.37 Particle size distribution of LaF$_3$: Ce at 10% nanocrystals with DI- water

3.4.2 PSD for samples prepared using DI- chitosan
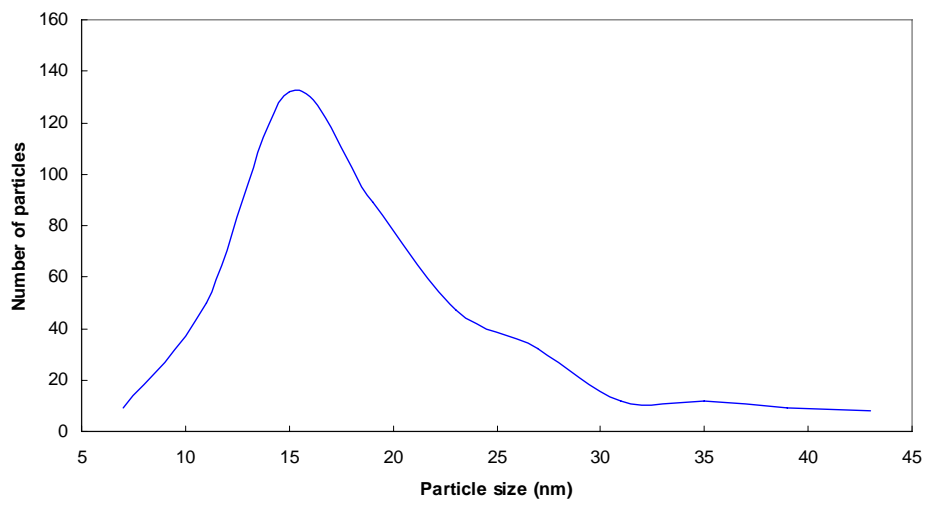
Fig 3.38 Particle size distribution of LaF$_3$: Ce at 0% nanocrystals with DI- chitosan
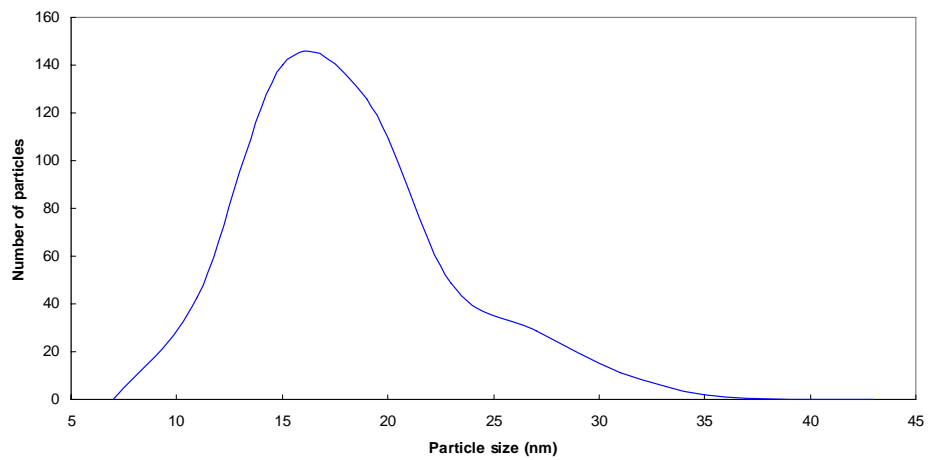
Fig 3.39 Particle size distribution of LaF$_3$: Ce at 1% nanocrystals with DI- chitosan
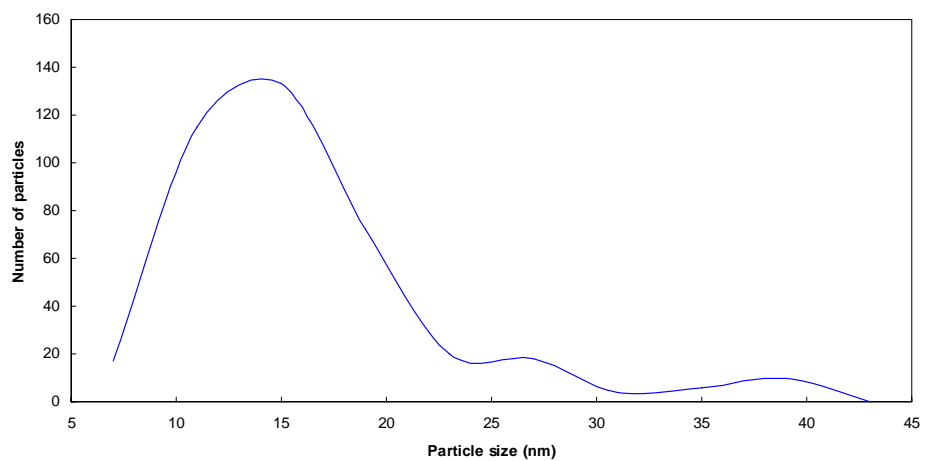
Fig 3.40 Particle size distribution of LaF$_3$: Ce at 3% nanocrystals with DI- chitosan
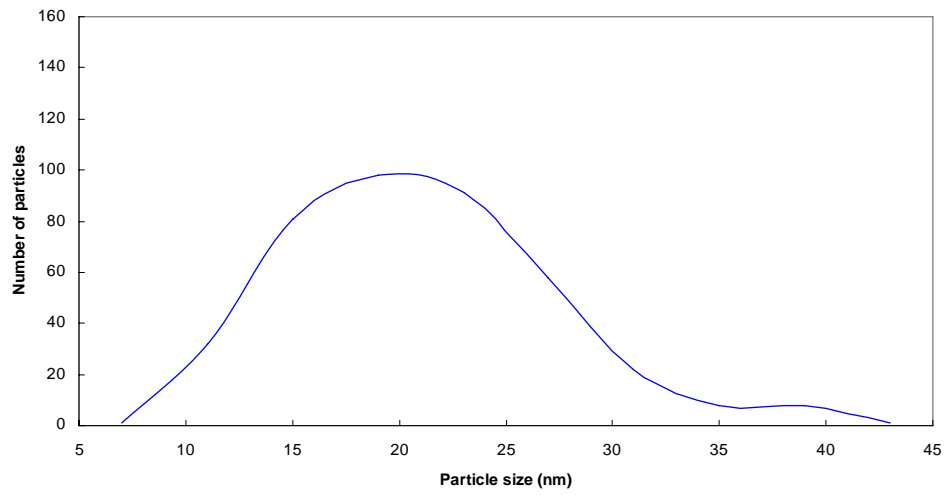
Fig 3.41 Particle size distribution of LaF$_3$: Ce at 5% nanocrystals with DI- chitosan
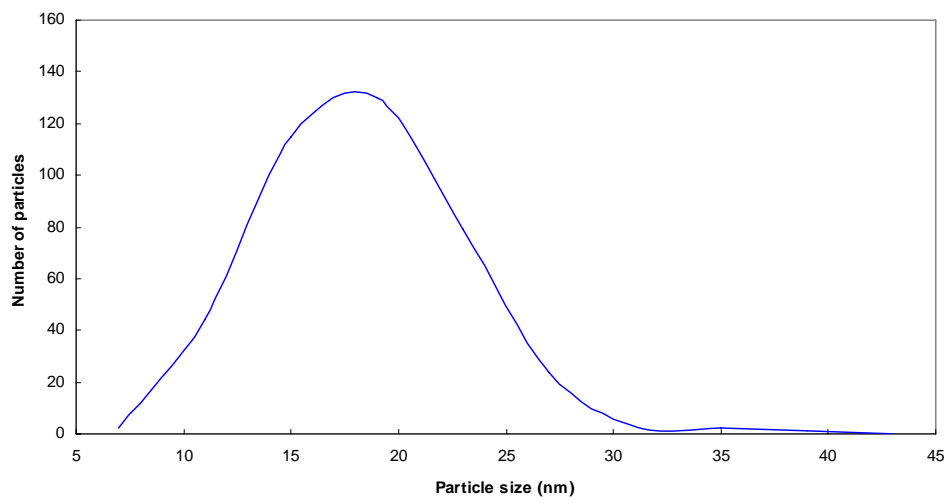
Fig 3.42 Particle size distribution of LaF$_3$: Ce at 10% nanocrystals with DI- chitosan

Chapter 4

Fluorescence Testing

4.1 Fluorescence Measurement

There are several factors that affect whether a compound will fluoresce or not, such as temperature of the environment, pH of the solution, concentrations of fluorophores, and sample internal properties. Here, we will focus our investigation on the influence on fluorescent properties induced by a few parameters, including changing the Ce dopant concentration, changing the fluorophore concentration, and using DI- water as solvent or DI- chitosan as deagglomerater in the synthesis of the LaF_3: Ce nanocrystals.

4.2 Measurement Apparatus

Current spectrofluorometers are capable of recording both excitation and emission spectra. An emission spectrum is the wavelength distribution of an emission measured at a single constant excitation wavelength. An excitation spectrum is the dependence of

emission intensity, measured at a single emission wavelength, upon scanning the excitation wavelength. Such spectra can be presented on either a wavelength scale or a wave number scale. Alternatively, light of a given energy can be described in terms of its wavelength λ, frequency ν, or wave number $\bar{\nu}$. The usual units for wavelength are nanometers, and wave numbers are given in units of cm^{-1}. Wavelengths and wave numbers are easily interconverted by taking the reciprocal of each value. However, most commercially available instrumentation yields spectra on the wavelength scale, and such spectra are more familiar and thus easier to interpret visually.

For an ideal instrument, the directly recorded emission spectra would represent the photon emission rate or power emitted at each wavelength, over a wavelength interval determined by the slit widths and dispersion of the emission monochromator. Similarly, the excitation spectrum would represent the relative emission of the fluorophores at each excitation wavelength. For most fluorophores the quantum yield and emission spectra are independent of excitation wavelength. As a result, the excitation spectrum of a fluorophore can be superimposed on its absorption spectrum (Molecular Devices).

However, such identical absorption and excitation spectra are rarely observed since excitation intensity is different at each wavelength. Even under ideal circumstances such correspondence of the excitation and absorption spectra requires the presence of only a single type of fluorophore, and the absence of other complicating factors, such as a nonlinear response resulting from a high optical density of the sample or the presence of other chromophores in the sample. Emission spectra recorded on different instruments

can be different because of the wavelength-dependent sensitivities of the instruments (

Molecular Devices).

Fig 4.1 shows a schematic diagram of a generic spectrofluorometer: this instrument has a xenon lamp as a source of exciting light. Such lamps are generally useful because of their high intensity at all wavelengths ranging upward from 250 nm. The instrument shown is equipped with monochromators to select both the excitation and emission wavelengths. Both monochromators are motorized to allow automatic scanning of wavelength. The fluorescence is detected with photomultiplier tubes and quantified with the appropriate electronic devices. The output is usually presented in graphical form and stored digitally.
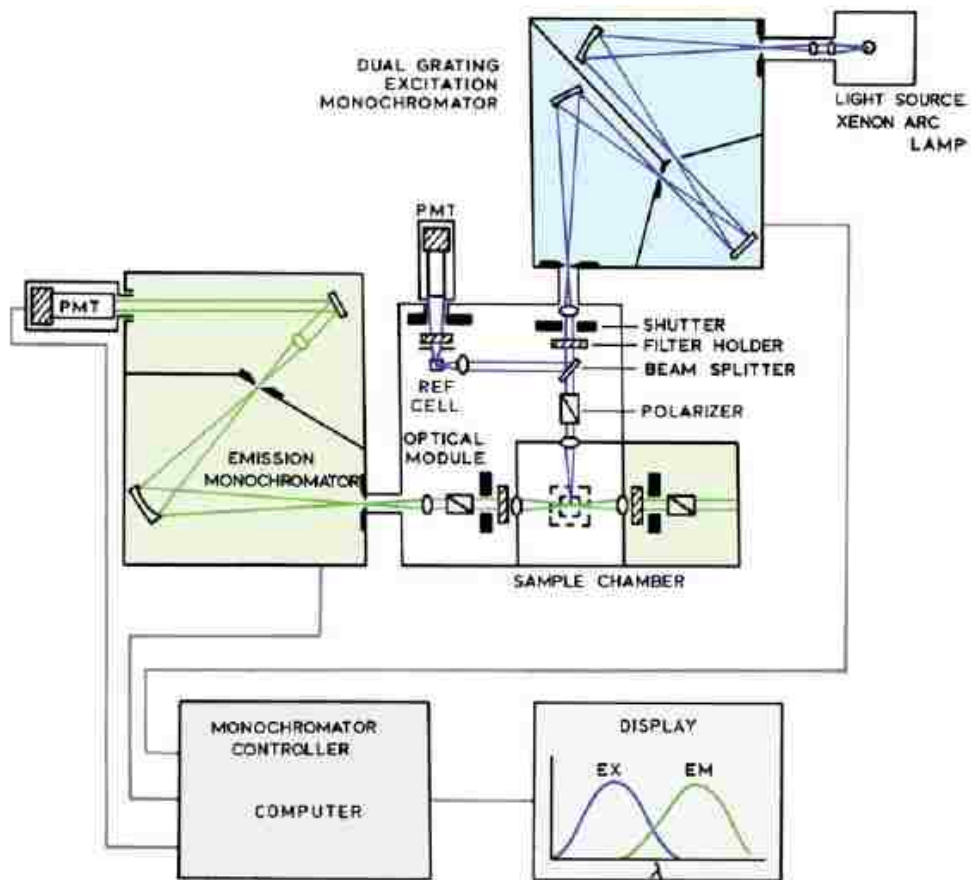
Fig 4.1 Schematic diagram of a spectrofluorometer, from (Molecular Devices)

In an ideal case, the recorded excitation and emission spectra would represent the relative

photon intensity per wavelength interval. To obtain such "corrected" emission spectra,

individual components must have the following characteristics (Lakowicz 2006):

1. The light source must yield a constant photon output at all wavelengths;

2. The monochromator must pass photons of all wavelengths with equal efficiency;

3. The monochromator efficiency must be independent of polarization; and

4. The detector (photomultiplier tube) must detect photons

Unfortunately, light sources, monochromators, and photomultiplier tubes with such ideal characteristics are not available. As a result, one is forced to compromise on the selection of components and to correct for the nonideal response of the instrument.

Measurements of photoluminescent excitation and emission spectra were performed using a Varian Cary Eclipse Fluorescence Spectrophotometer (Fig 4.2). The LaF$_3$: Ce nanocrystals solution with concentrations at 0.3 g/L and 1 g/L were carefully prepared and fully sonicated. The solution remains clear and homogeneous at 0.3 g/L, while a little bit white at 1 g/L. The excitation spectra were obtained by setting excitation mode as "Zero order excitation scanning" and slit value as "2.5", ranging from 200 nm to 900 nm.
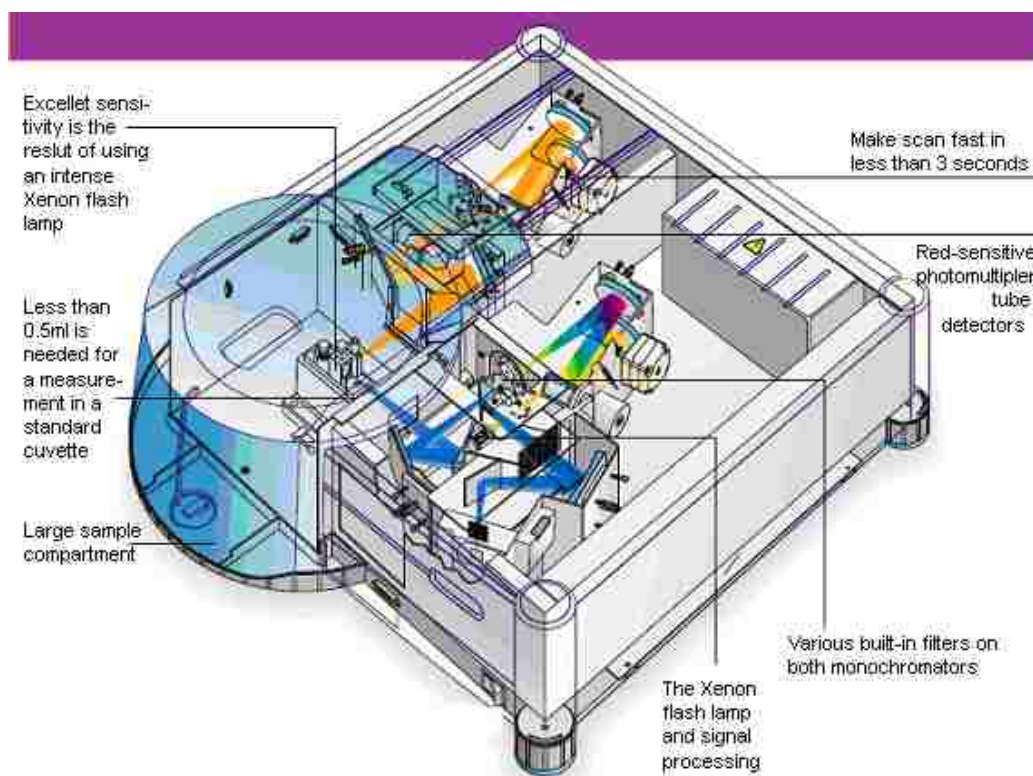
Fig 4.2 Varian Cary Eclipse Fluorescence Spectrophotometer (Varian).

4.3 Fluorescence results

4.3.1 Excitation spectra

The fluorescence tests were carried out for both excitation and emission spectra for LaF_3: Ce nanocrystals at different Ce concentrations and in different solution concentrations. In this chapter, the effect of Ce concentrations (0%, 1%, 5% and 10%) on excitation and emission spectra would be primarily studied.

Figs 4.3- 4.6 show the room temperature excitation spectra of LaF_3: Ce^{3+} doped with different Ce percentages (0%, 1%, 5% and 10%) with different solvents in 0.3 g/L solution and 1.0 g/L solution, respectively. It can be seen that the excitation spectra for Ce^{3+} contain five bands which are centered in 250 nm, 351 nm, 391 nm, 531 nm and 611 nm for all cases. All spectra look quite similar. Their shapes and positions show little changes with the increase of Ce-doped concentration. It is also noticed that when using DI- water, the excitation intensity of the LaF_3: Ce nanocrystals increases with the increase of Ce concentration. When LaF_3 NCs were doped with 5% Ce^{3+}, the intensity reaches the maximum, and then decreases with the further increase of Ce concentration. No obvious shift of the excitation peaks and trends were observed as solution concentration was changed from 0.3 g/L to 1.0 g/L. In the other hand, when using DI- chitosan, it can be seen that LaF_3: Ce^{3+} doped at 1% shows the highest intensity. As Ce concentration increases to 5%, the excitation intensity decreases. And when dopant concentration reaches 10%, the intensity touches the bottom. Compared to excitation spectra with DI- chitosan in 1.0 g/L, excitation spectra in 0.3 g/L remain the same intensity trend with different Ce concentrations.
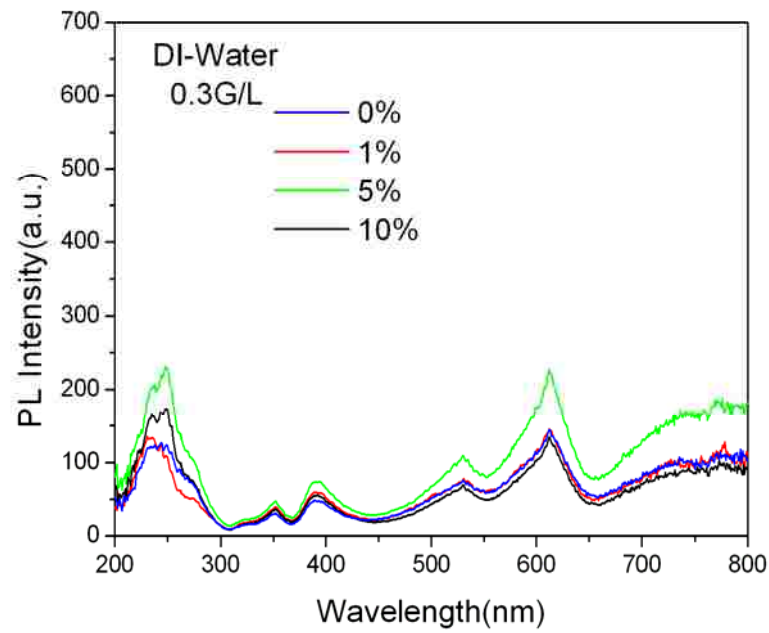
Fig 4.3 PL excitation spectra for LaF$_3$: Ce^{3+} NCs with DI- water at 0.3 g/L at different Ce concentrations.
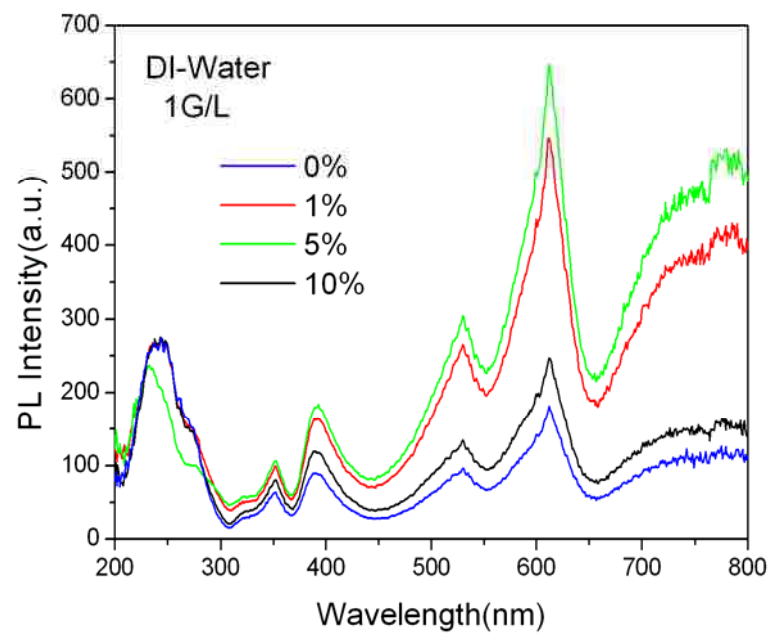
Fig 4.4 PL excitation spectra for LaF$_3$: Ce^{3+} NCs with DI- water at 1.0 g/L at different Ce concentrations.
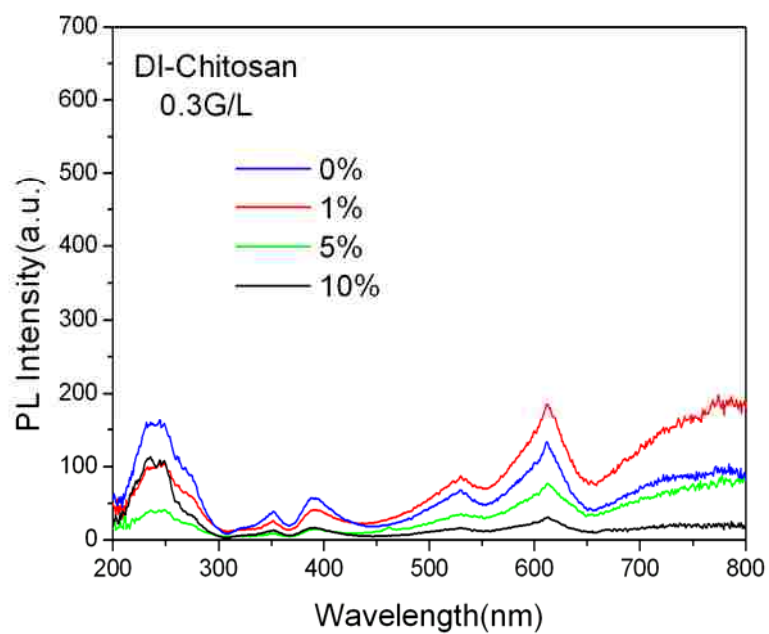
Fig 4.5 PL excitation spectra for LaF$_3$: Ce^{3+} NCs with DI- chitosan at 0.3 g/L at different Ce concentrations.
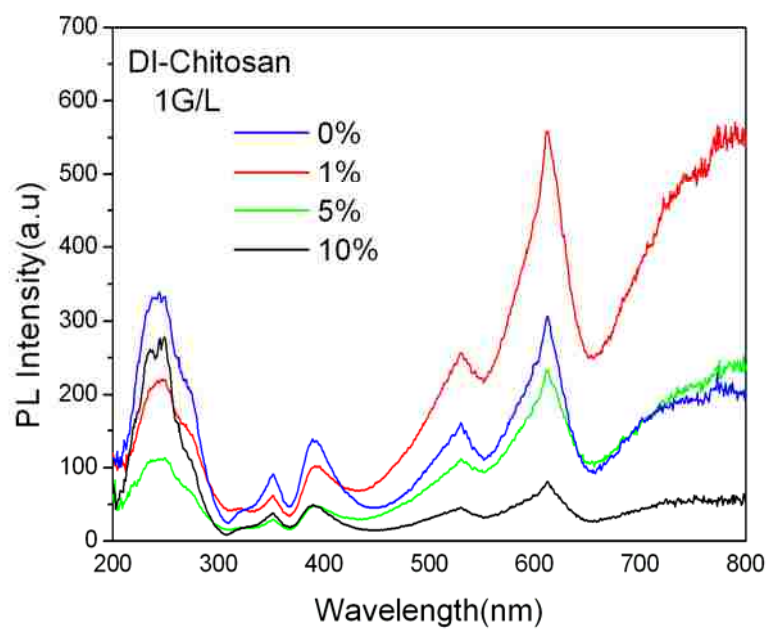
Fig 4.6 PL excitation spectra for LaF$_3$: Ce^{3+} NCs with DI- chitosan at 1.0 g/L at different Ce concentrations.

61

4.3.2 Emission spectra

Figs 4.7 to 4.10 show the emission spectra of LaF_3: Ce at different Ce concentrations. To investigate emission spectra conveniently, three emission patterns were plotted in one. In emission patterns, emission wavelength from 200 nm~ 675 nm was excited at 250 nm. The emission wavelength from 675 nm~ 725 nm was excited at 351 nm, and wavelength from 725 nm~ 850 nm was excited at 391nm. However, no emission spectra obtained when excited at 531 nm or 611 nm. For all images below (Fig 4.7-Fig 4.10), one can observe that the emission spectra consist of a broad band from 250 nm to 400 nm with a maximum at 305 nm, and three sharper peaks centered at 499 nm, 700 nm, and 782 nm.
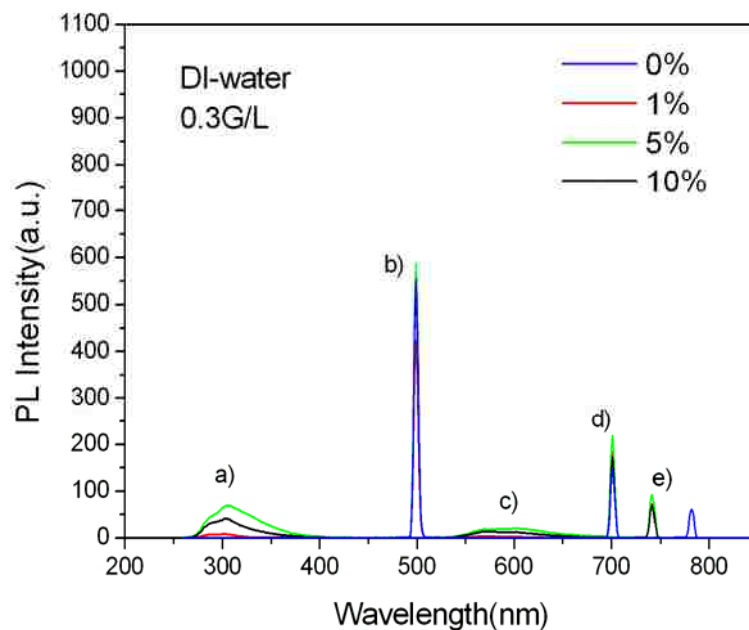
Fig 4.7 PL emission spectra of LaF_3: Ce^{3+} NCs with DI- water at 0.3 g/L with different Ce concentrations

Fig 4.7 shows the photoluminescent emission spectra of LaF_3: Ce nanocrystals with different Ce concentrations (0%, 1%, 5% and 10%). It shows that the emission intensity

increases as the Ce concentration increases from 0% to 5%. After this, emission intensity
falls down when 10% Ce ions were doped.
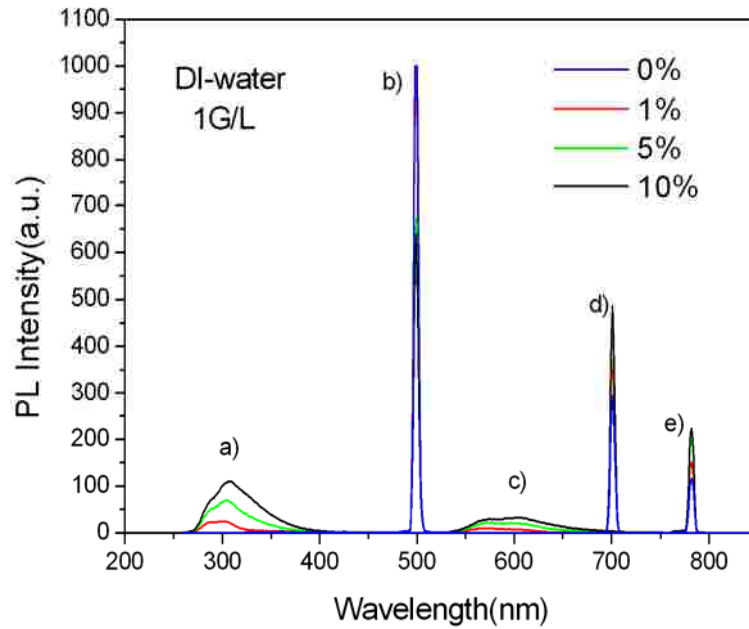
Fig 4.8 PL emission spectra of LaF$_3$: Ce^{3+} NCs with DI- water at 1.0 g/L with different Ce concentrations.

From Fig 4.8, it was found that the emission spectra intensity increases as the Ce
concentration increases except the peak at 500 nm.
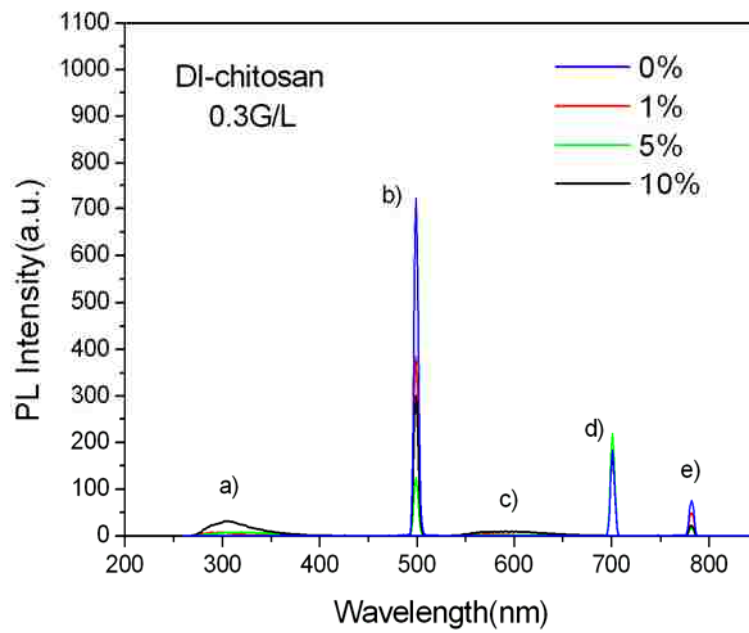
Fig 4.9 PL emission spectra of LaF$_3$: Ce^{3+} NCs with DI- chitosan at 0.3 g/L with different Ce

concentrations.

In Fig 4.9, it is found that emission spectra shows no trend when $\lambda_{ex} = 250$ nm. However,

when $\lambda_{ex} = 351$ nm and $\lambda_{ex} = 391$ nm, the emission spectra decreases as the Ce dopant

percentage increases.
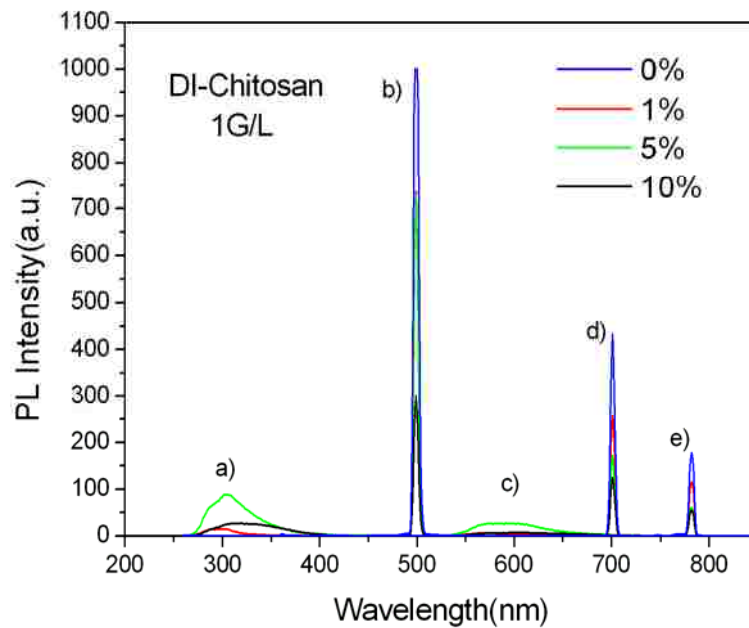
Fig 4.10 PL emission spectra of LaF$_3$: Ce^{3+} NCs with DI- water at 1.0 g/L with different Ce concentrations.

In Fig 4.10, it is found that emission intensity decreases as Ce ions increases.

4.3.3 Stokes shift

Figs 4.11 to 4.14 present the information about excitation and emission spectra in same image. In excitation spectra, the peaks marked 1), 2) and 3) represent the excitation peaks obtained from zero order excitation scanning. Their values were very close to 250 nm, 351 nm and 391 nm, respectively. The peaks beyond 391 nm were not labeled here because there were no corresponding emission spectra obtained upon testing. In emission spectra, the peaks marked a), b) and c) were excited at 250 nm. And the emission peaks marked d) and e) were excited at 351 nm and 391 nm, respectively.

To calculate the Stokes shift, peaks 1), 2) and 3) were chosen to obtain excitation wavelengths, and peaks b), d) and e) were chosen to achieve emission wavelengths. The Stokes shift was calculated by $(hc/\lambda_{ex} - hc/\lambda_{em})$ (J).
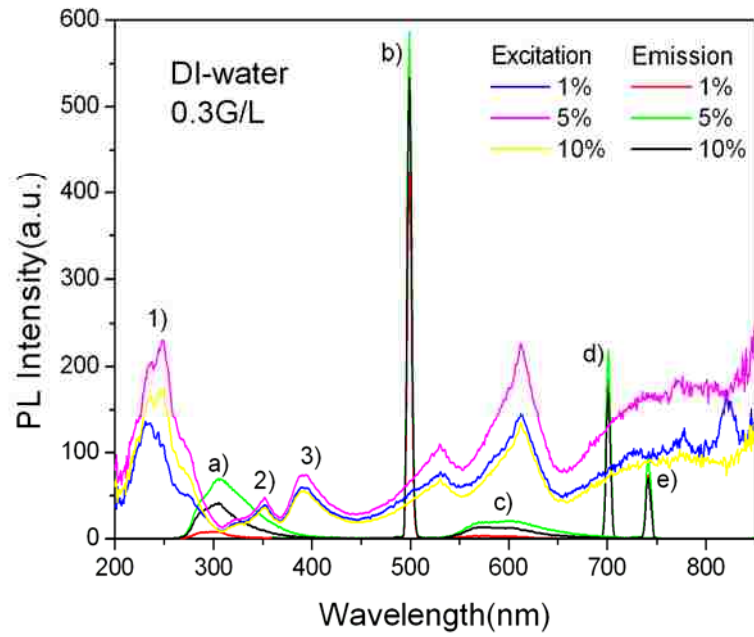
Fig 4.11 PL excitation and emission spectra of LaF_3: Ce^{3+} NCs with DI- water at 0.3 g/L
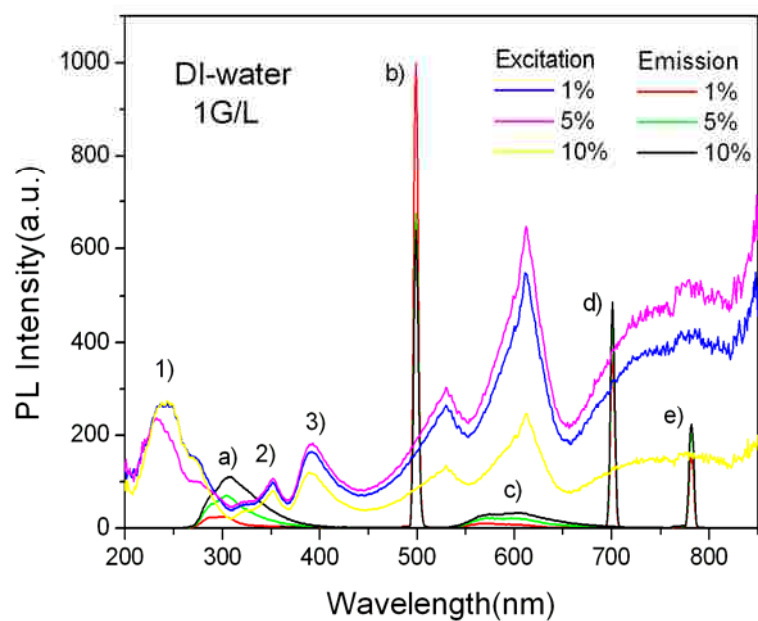
Fig 4.12 PL excitation and emission spectra of LaF$_3$: Ce^{3+} NCs with DI- water at 1.0 g/L
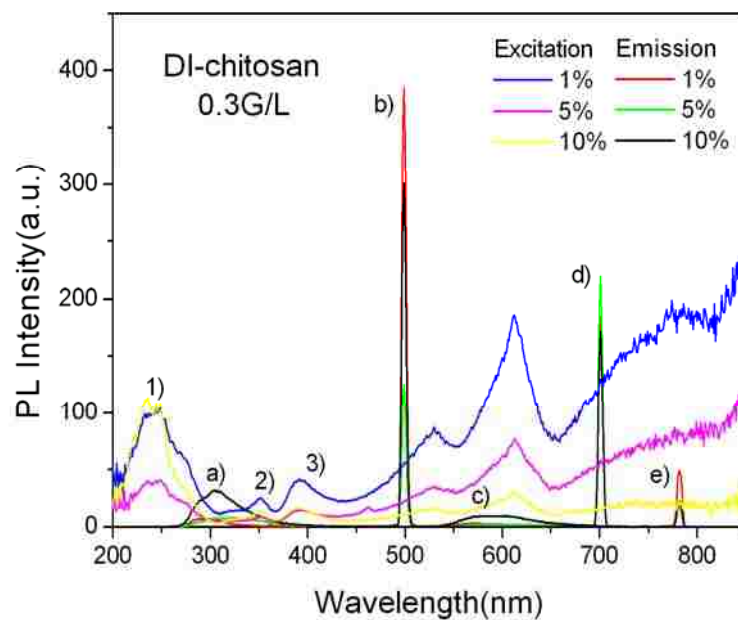
Fig 4.13 PL excitation and emission spectra of LaF$_3$: Ce^{3+} NCs with DI- chitosan at 0.3 g/L
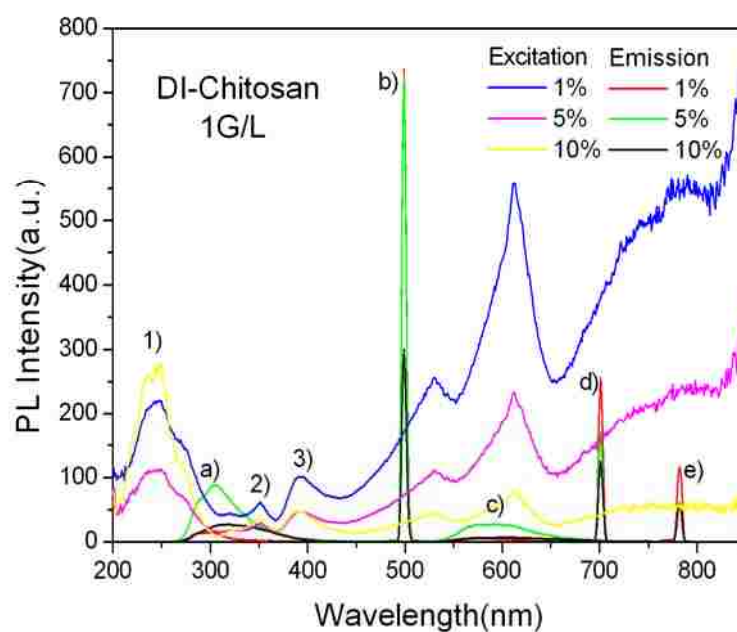
Fig 4.14 PL excitation and emission spectra of LaF$_3$: Ce^{3+} NCs with DI- chitosan at 1.0 g/L

Table 4.1 Stokes shift table of DI- water in 0.3 g/L solution

DI-water 0.3 g/L	Excitation wavelength λ$_{ex}$ (nm)	Emission Wavelength λ$_{em}$ (nm)	Stokes Shift ΔE = (hc/λ$_{ex}$ − hc/λ$_{em}$) (10^{-19} J)
1%	234.92 ± 1.5	499.16 ± 1.5	4.477 ± 0.066
5%	247.88 ± 1.5	499.16 ± 1.5	4.034 ± 0.060
10%	250.00 ± 1.5	499.16 ± 1.5	3.966 ± 0.060
1%	351.40 ± 1.5	700.89 ± 1.5	2.819 ± 0.030
5%	351.40 ± 1.5	700.84 ± 1.5	2.819 ± 0.030
10%	351.40 ± 1.5	700.83 ± 1.5	2.819 ± 0.030
1%	391.90 ± 1.5	742.45 ± 1.5	2.393 ± 0.025
5%	391.90 ± 1.5	742.45 ± 1.5	2.393 ± 0.025
10%	390.78 ± 1.5	742.46 ± 1.5	2.408 ± 0.025

Table 4.2 Stokes shift table of DI- water in 1.0 g/L solution

DI-water 1.0 g/L	Excitation wavelength λ_{ex} (nm)	Emission Wavelength λ_{em} (nm)	Stokes Shift $\Delta E = (hc/\lambda_{ex} - hc/\lambda_{em})$ (10^{-19} J)
1%	241.89± 1.5	499.16 ± 1.5	4.233 ± 0.063
5%	233.80 ± 1.5	499.16 ± 1.5	4.517 ± 0.066
10%	243.01 ± 1.5	499.16 ± 1.5	4.195 ± 0.062
1%	351.40 ± 1.5	700.83 ± 1.5	2.819 ± 0.030
5%	351.40 ± 1.5	700.83 ± 1.5	2.819 ± 0.030
10%	351.39 ± 1.5	700.83 ± 1.5	2.819 ± 0.030
1%	390.78 ± 1.5	781.56 ± 1.5	2.542 ± 0.024
5%	391.89 ± 1.5	781.56 ± 1.5	2.527 ± 0.024
10%	390.79 ± 1.5	781.56 ± 1.5	2.542 ± 0.024

Table 4.3 Stokes shift table of DI- chitosan in 0.3 g/L solution

DI-chitosan 0.3 g/L	Excitation wavelength λ_{ex} (nm)	Emission Wavelength λ_{em} (nm)	Stokes Shift $\Delta E = (hc/\lambda_{ex} - hc/\lambda_{em})$ (10^{-19} J)
1%	250.00 ± 1.5	499.16 ± 1.5	3.966 ± 0.060
5%	247.48 ± 1.5	498.04 ± 1.5	4.038 ± 0.061
10%	248.88 ± 1.5	499.16 ± 1.5	4.002 ± 0.060
1%	351.40 ± 1.5	700.84 ± 1.5	2.819 ± 0.030
5%	350.28 ± 1.5	700.84 ± 1.5	2.837 ± 0.030
10%	350.28 ± 1.5	700.84 ± 1.5	2.837 ± 0.030
1%	390.78 ± 1.5	781.56 ± 1.5	2.542 ± 0.024
5%	391.90 ± 1.5	781.56 ± 1.5	2.527 ± 0.024
10%	390.01 ± 1.5	782.96 ± 1.5	2.556 ± 0.024

Table 4.4 Stokes shift table of DI- chitosan in 1.0 g/L solution

DI-chitosan 1.0 g/L	Excitation wavelength λ_{ex} (nm)	Emission Wavelength λ_{em} (nm)	Stokes Shift $\Delta E = (hc/\lambda_{ex} - hc/\lambda_{em})$ (10^{-19} J)
1%	247.48 ± 1.5	499.16 ± 1.5	4.047 ± 0.061
5%	245.25 ± 1.5	499.16 ± 1.5	4.120 ± 0.061
10%	248.88 ± 1.5	499.16 ± 1.5	4.002 ± 0.060
1%	351.40 ± 1.5	700.84 ± 1.5	2.819 ± 0.030
5%	351.40 ± 1.5	700.83 ± 1.5	2.819 ± 0.030
10%	351.39 ± 1.5	700.84 ± 1.5	2.819 ± 0.030
1%	390.78 ± 1.5	781.56 ± 1.5	2.542 ± 0.024
5%	391.89 ± 1.5	781.56 ± 1.5	2.527 ± 0.024
10%	391.89 ± 1.5	781.56 ± 1.5	2.527 ± 0.024

Tables 4.1 to 4.4 show Stokes shift decreased as more Ce ions were doped in most cases. In other words, higher impurity in nanoparticles induced by higher dopant concentration decreased Stokes shift, and subsequently decreased energy loss and improved their fluorescence properties.

Chapter 5

Discussion

5.1 Discussion

To investigate LaF$_3$: Ce nanoparticle fluorescence, the effects of different Ce

concentrations, the type of solvents/ deagglomerater, and the fluorophore concentrations

will be analyzed. In Chapter 4, we shed some light on the effect of varying Ce dopant

concentrations on both emission, excitation spectra and on the Stokes shift. In this

chapter, we will focus on the other two factors: the effect of the solvent/ deagglomerater

used in synthesis and the effect of different fluorophore concentrations.

5.1.1 Comparison of excitation

1) *Effects of DI- water solvent and DI- chitosan deagglomerater*
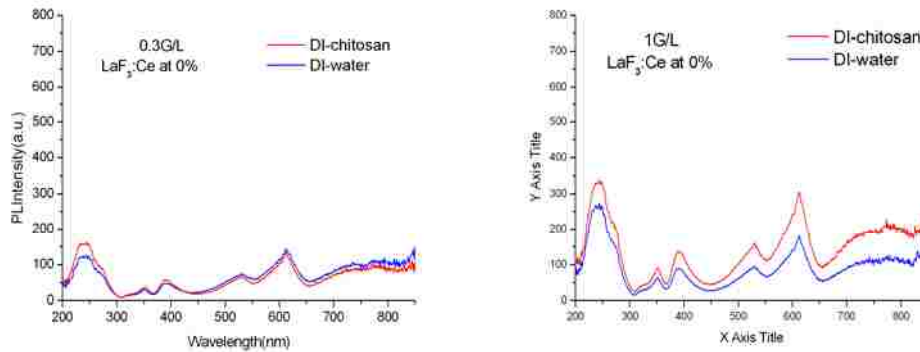
Fig 5.1 Excitation spectra (λ = 850 nm) of 0% Ce^{3+} doped LaF_3 nanocrystals in 0.3 g/L solution (left) and in 1.0 g/L solution (right), respectively

Fig 5.2 Excitation spectra (λ = 850 nm) of 1% Ce^{3+} doped LaF_3 nanocrystals in 0.3 g/L solution (left) and in 1.0 g/L solution (right), respectively

Fig 5.3 Excitation spectra (λ = 850 nm) of 5% Ce^{3+} doped LaF_3 nanocrystals in 0.3 g/L solution (left) and in 1.0 g/L solution (right), respectively

Fig 5.4 Excitation spectra (λ = 850 nm) of 10% Ce^{3+} doped LaF_3 nanocrystals in 0.3 g/L solution (left) and in 1.0 g/L solution (right), respectively

Figs 5.1 to 5.4 show how DI- water solvent and DI- chitosan deagglomerater affected the LaF_3 NCs excitation spectra when doped with 0%, 1%, 5% and 10% Ce ions in 0.3 g/L or 1.0 g/L solvent. It can be seen that in DI- water case, when 0% or 1% Ce ions are doped with LaF_3 NCs, solution with DI- water shows lower intensity than with DI- chitosan. However, as the Ce concentration increases to 5% and 10%, respectively, the solution using DI- water shows higher excitation intensity than using DI- chitosan. The same trend occurs in both 0.3 g/L and in 1.0 g/L cases.

The resulting intensity difference indicates that when Ce concentration is lower than 5%, the solution with DI- chitosan can emit more fluorescence; while the Ce concentration keeps increasing to 10%, solution with DI- water would give higher excitation spectra intensity.

73

2) Effects of the LaF₃: Ce fluorophore concentration
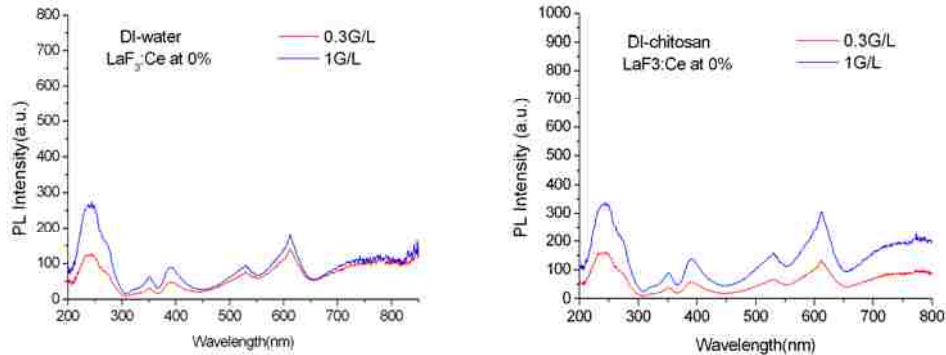
Fig 5.5 Excitation spectra (λ = 850 nm) of 0% Ce³⁺ doped LaF₃ nanocrystals with DI-water (left) and with DI– chitosan (right), respectively.

Fig 5.6 Excitation spectra (λ = 850 nm) of 1% Ce³⁺ doped LaF₃ nanocrystals with DI-water (left) and with DI- chitosan (right), respectively.

Fig 5.7 Excitation spectra (λ = 850 nm) of 5% Ce³⁺ doped LaF₃ nanocrystals with DI-water (left) and with DI- chitosan (right), respectively.

Fig 5.8 Excitation spectra ($\lambda = 850$ nm) of 10% Ce^{3+} doped LaF$_3$ nanocrystals with DI-water (left) and with DI- chitosan (right), respectively.

Figs 5.5- 5.8 reveal the effects of different fluorophore concentrations on LaF$_3$: Ce NCs excitation spectra. One can notice that when other conditions are kept identical, 1.0 g/L solution always results in higher intensities than 0.3 g/L solutions. This indicates that higher solution concentration can generate higher emission intensity.

5.1.2 Comparison of emission

To compare the nanoparticles emission spectra conveniently, three different emission spectra are plotted in one pattern. From the excitation scanning, we know all of them can be excited at 250 nm, 351 nm, and 391 nm. The emission wavelengths ranging from 200 nm to 675 nm was excited at 250 nm. The emission wavelength at 650 nm~ 725 nm was excited at 351nm. Additionally, the wavelength at 725 nm~ 850 nm was excited at 391 nm.

1) Effects of DI- water solvent and DI- chitosan deaggolmerater on the emission spectra
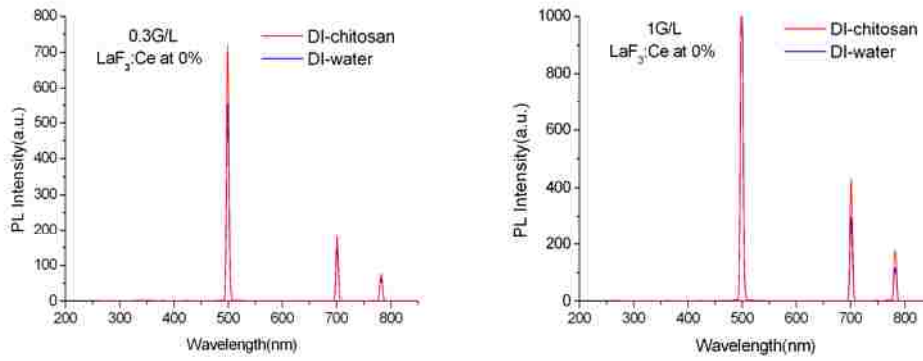
Fig 5.9 Emission spectra of 0% Ce^{3+} doped LaF_3 nanocrystals in 0.3 g/L solution (left) and in 1.0 g/L solution (right), respectively
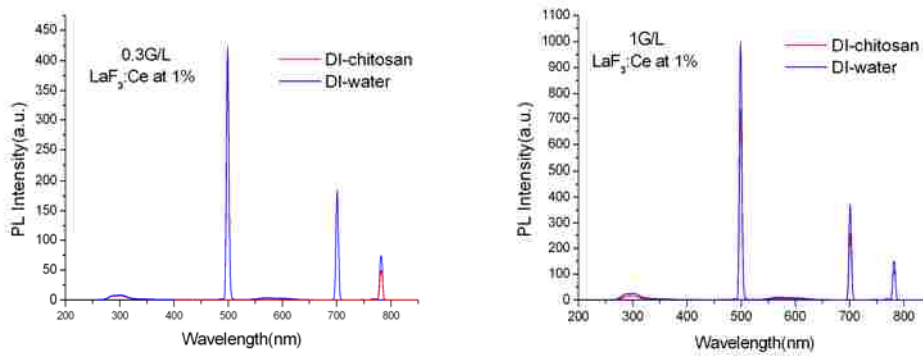
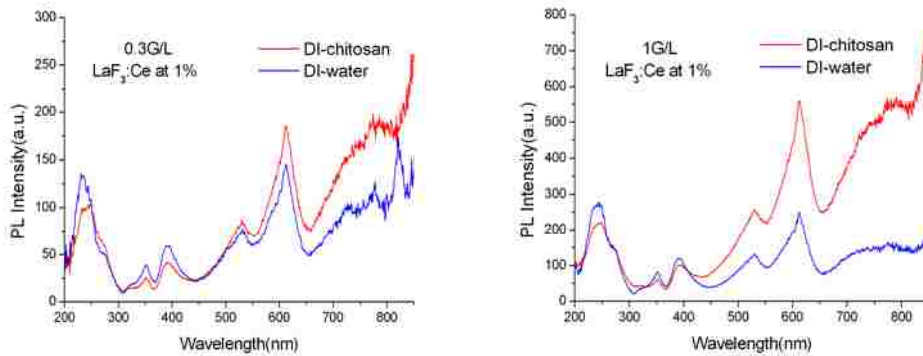**Fig 5.10** Emission spectra of 1% Ce^{3+} doped LaF_3 nanocrystals in 0.3 g/L solution (left) and in 1.0 g/L solution (right), respectively

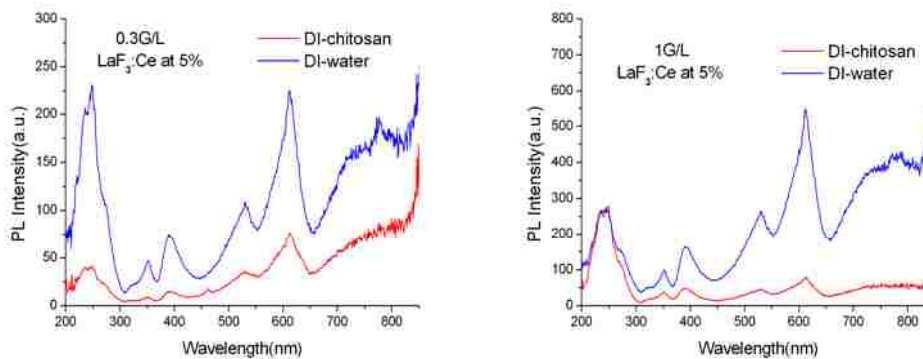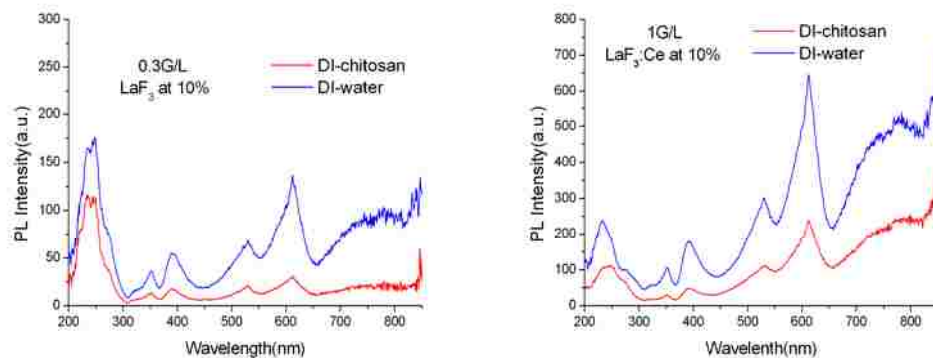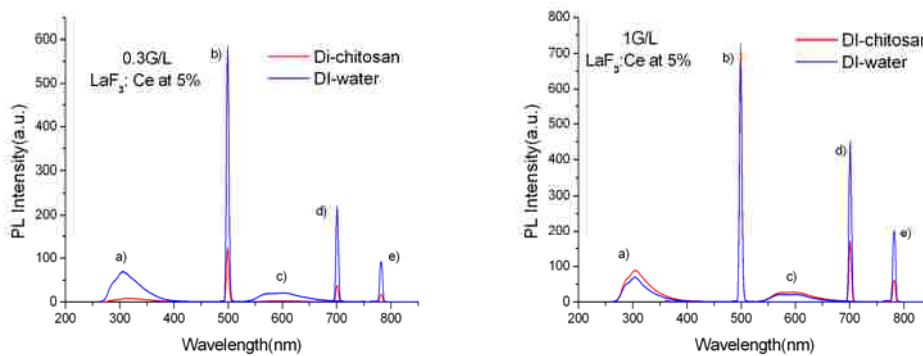**Fig 5.11** Emission spectra of 5% Ce^{3+} doped LaF_3 nanocrystals in 0.3 g/L solution (left) and in 1.0 g/L solution (right), respectively
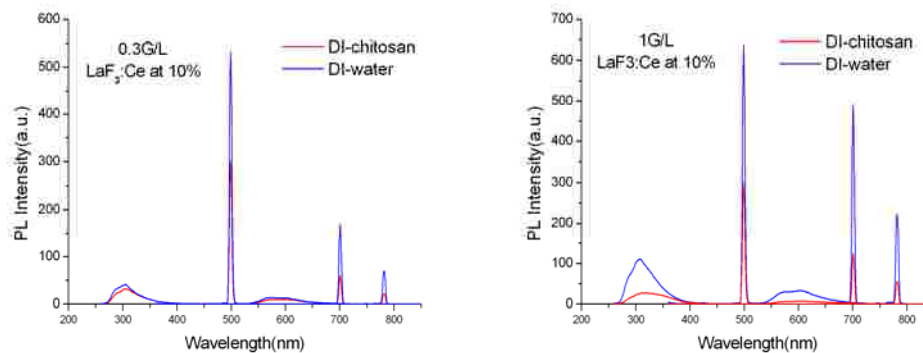
Fig 5.12 Emission spectra of 10% Ce^{3+} doped LaF_3 nanocrystals in 0.3 g/L solution (left) and in 1.0 g/L solution (right), respectively

As can be seen from Fig 5.9 to Fig 5.12, solutions of LaF_3 nanocrystals doped with 1%, 5% and 10% with DI- water generate higher intensity than those with DI- chitosan when we keep other parameters identical. It shows that LaF_3: Ce^{3+} nanocrystals which use DI- water as solvent can provide better fluorescent properties than using DI- chitosan deagglomerater. Instead, adding chitosan in synthesis quenches the nanoparticle fluorescence.

One can also observe from the particles size distribution figures for samples with chitosan (Figs 3.38 to3.42) and those for DI- water (Figs 3.33 to 3.37) that the NCs in the chitosan possess more relatively small particles than those in DI- water solvent. Samples with smaller size would possess higher surface area and more defects. These defects will lead to more nonradioactive decay on the surface of smaller crystals and thus will reduce the luminescence efficiency (Zhu et al. 2007). Similar observation was cited in the work of Li et al., (2008), where coating CeF_3: Tb^{3+} with LaF_3 shells would increase the distance between the luminescent lanthanide ions and then decrease the surface quencher thus reducing the nonradioactive pathways.

Furthermore, while the main use of chitosan is to deagglomerate NCs, it plays a negative role in hampering the emission intensity. Such negative behavior can be attributed to the high content of oxygen in chitosan which acts as an external quencher.

2) Effect of different fluorophore concentrations on the emission spectra
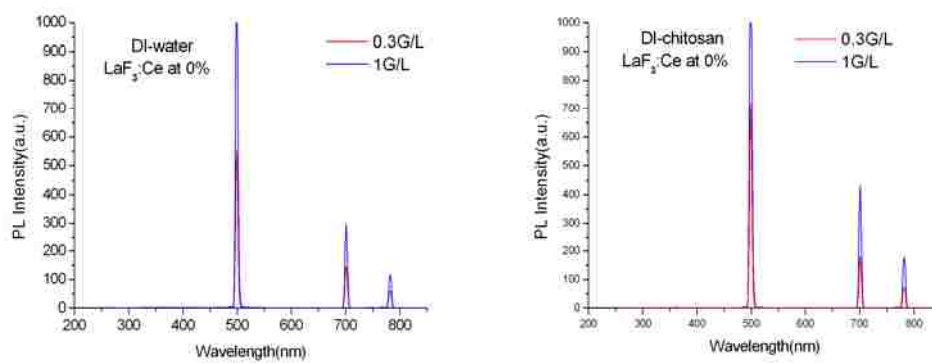
Fig 5.13 Emission spectra of 0% Ce^{3+} doped LaF_3 nanocrystals with DI-water (left) and with DI-chitosan (right), respectively
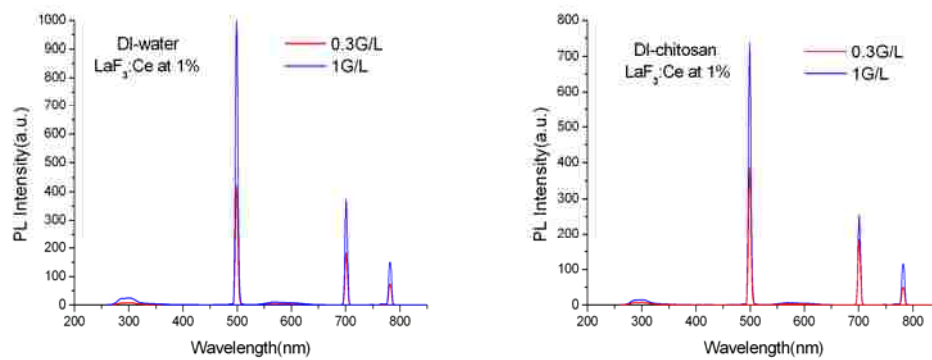
Fig 5.14 Emission spectra of 1% Ce^{3+} doped LaF_3 nanocrystals with DI-water (left) and with DI-chitosan (right), respectively
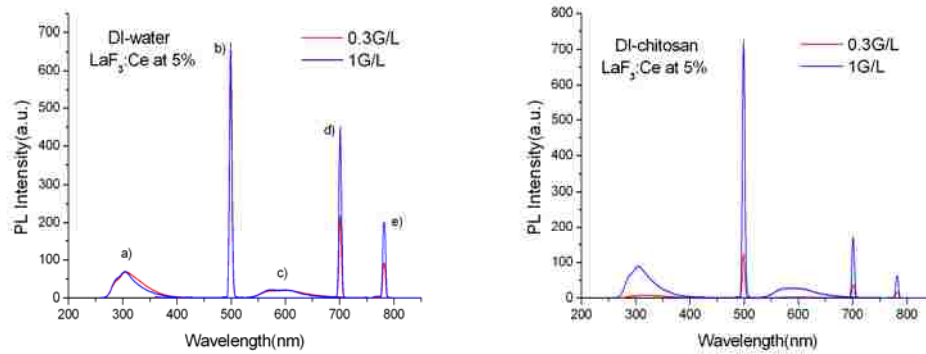
Fig 5.15 Emission spectra of 5% Ce^{3+} doped LaF_3 nanocrystals with DI-water (left) and with DI-chitosan (right), respectively
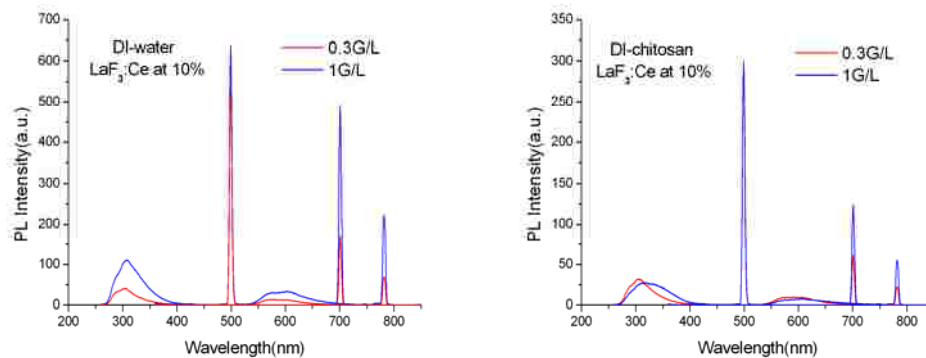
Fig 5.16 Emission spectra of 10% Ce^{3+} doped LaF_3 nanocrystals with DI-water (left) and with DI-chitosan (right), respectively

Figs 5.13 - 5.16 reveal the effects of different fluorophore concentrations on LaF_3: Ce NCs emissions spectra. One can notice that when other conditions are kept the same, 1.0 g/L solution always generates higher intensity than 0.3 g/L. The fact that this result agrees well with the trend from Figs 5.5 to 5.8, testifies that the emission intensity is proportional to the amplitude of the excitation spectrum at the excitation wavelength. And it also indicates that higher solution concentration can generate higher emission intensity.

Chapter 6

Conclusions and future work

6.1 Conclusions

In summary, the highly water-soluble lanthanide-doped LaF_3 have been synthesized in aqueous solutions: methanol, DI- water and DI- chitosan. The LaF_3 nanocrystals with methanol have a relatively smaller mean size of about 7 nm, but offer agglomeration. Those nanoparticles with DI- water and DI- chitosan are in a mean size of about 19 nm and 17 nm, respectively, with a nearly hexagonal shape. In addition, they have high crystallinity and well dispersion in solvents. Through photoluminescence tests, the nanoparticles with DI- water /DI- chitosan exhibited strong luminescence in visible regions.

Effects of parameters including Ce concentrations, DI- water and DI- chitosan used in the synthesis as well as fluorophore concentrations on nanoparticles fluorescence were investigated. We summarize the major findings based on these parameters as follows:

- Solutions with higher LaF$_3$: Ce fluorophore concentration provide stronger fluorescence than those with lower solution concentration. This is because solutions at higher concentration contain more nanoparticles which can absorb and emit more photons and generate more fluorescence.

- A solution with DI- water provides stronger fluorescence than that with DI- chitosan, which is possibly due to the solution's pH value and particle size. As mentioned before, during the process to synthesize nanocrystals with DI- chitosan, pH of the solution was adjusted to 6.5 with diluted ammonia solution or acetic acid in order to prevent nanoparticles aggregation and precipitation. But the fact that pH of the solution tested by pH paper was not accurate enough may also affect their photoluminescence. Furthermore, nanoparticles size affected fluorescence as well. The observation from PSD suggests that nanoparticles with DI- water offer relatively larger particles size than those with DI- chitosan, and subsequently have less surface area and less defects leading to stronger photoluminescence.

- One may think that higher Ce concentration provides higher fluorescence. However, the extra fluorescence obtained decrease as dopant amount increases due to concentration quenching effect. The fluorescent tests give us the information about the maximum quantum yield. For DI- water, quantum yield would increase when Ce concentration reaches 5%, and then fall down. While

with DI- chitosan, nanoparticles quantum yield reaches maximum at 1% and decreases when doping more Ce ions.

Besides the factors mentioned above, some environmental conditions may also play a role of affecting fluorescent results, for instance, temperature, light exposure and so on.

6.2 Future work

To date, little work has been done about LaF_3: Ce nanocrystals. Further studies are currently underway to investigate LaF_3: Ce nanocrystals characterizations using other techniques such as X-ray fluorescence. Furthermore, different rare earth elements including Er, Eu, Pr and Sm are very promising alternative dopants to investigate using the same simple synthesis means as well.

To reduce the surface defects leading to nonradioactive decay, growth of a crystalline shell of inorganic material will be carried out in future work. These core/shell structures were shown as effective in enhancing the luminescence efficiency on CeF_3: Tb^{3+} @ LaF_3 (Core-Shell) nanoplates (Stouwdam et al. 2003; Wang et al. 2006 Chem. Mater.; Li et al. 2008). Several factors affecting fluorescence results need to be taken into account as well; for example, temperature of environment, pH of the solution, size of the sample, and samples store condition.

References

Beaurepaire, E., et al., *Functionalized fluorescent oxide nanoparticles: Artificial toxins for sodium channel targeting and imaging at the single-molecule level.* Nano Letters, 2004. **4**: p. 2079-83.

Bhagava, R.N.,and Gallagher, D., *Optical properties of manganese-doped nanocrystals of ZnS.* Physical Review Letters, 1994. **72**: p. 416-9.

Calvo, P., et al., *Novel hydrophilic chitosan-polyethylene oxide nanoparticles as protein carriers.* Journal of Applied Polymer Science, 1997. **63**: p. 125-32.

Cooke, D.W., et al., *Luminescent properties and reduced dimensional behavior of hydrothemally prepared Y_2SiO_5:Ce nanophpsphors.* Applied Physics Letters, 2006. **88**: p. 103108-11.

Molecular Devices, *Microplate Spectrofluoromter.*
<http://www.moleculardevices.com/pages/instruments/gemini.html>

Diamente, P. R., and Veggel, F. C. J. M. van, *Water-soluble Ln^{3+} Doped LaF_3 Nanopartilces: Retention of strong luminescence and potential as biolables.* Journal of Fluorescence, 2005. **15**: P. 543-51

Goosen, M. F. A., *Applications of chitan and chitosan.* First Edition, CRC Press, 1996

Hui, L. L., Lu, X. J., and Huang, L. P., *Luminescent properties of LuAG:Ce phosphors with different Ce contents prepared by a sol-gel combustion method.* Optical Materials, 2007. **29**: p. 1138-42.

Invitrogen, *Introduction to fluorescence techniques.*
<http://www.invitrogen.com/site/us/en/home/References/Molecular-Probes-The-Handbook/Introduction-to-Fluorescence-Techniques.html>

Jiang, C., Deng, P. Z., Zhang, J. Z., and Gan, F. X., *Radioluminescence of Ce^{3+} doped B_2O_3-SiO_2-Gd_2O_3-BaO glass.* Physics Letters A, 2004. **323**(3-4): p. 323-8.

Justel, T., Nikol, H., and Ronda, C., *New developments in the field of luminescent material for lighting and displays.* Angewandte Chemie International Edition, 1998. **37**: p. 3085-103.

Kitai, A.H., *Solid State Luminescence: Theory, materials and devices.* First Edition. Springer, New York, 1993.

Klink, I., et al., *Sensitized near-infrared luminescence from polydentate triphenylene-functionalized Nd^{3+}, Yb^{3+} and Er^{3+} complexes.* Journal of applied physics, 1999. **86**: p. 1181-5.

Kunar, M. N. V. R., *A review of chitin and chitosan applications.* Reactive and Functional Polymers, 2000. **46**: p. 1-27.

Metallium, *Lanthanide rare-earth metal element set.* <http://www.elementsales.com/set-re-1.htm>

Lakowicz, J.R., *Principles of Fluorescence Spectroscopy.* Third Edition. Springer, New York, 2006.

Li, C. X., et al., *LaF_3, CeF_3, CeF_3:Tb^{3+}, and CeF_3:Tb^{3+}@LaF_3 (Core−Shell) Nanoplates: Hydrothermal Synthesis and Luminescence Properties.* Journal of Physical Chemistry C, 2008. **112**(8): p. 2904-10.

Liu, Z.Y., et al, *One-Step fabrication and high photocatalytic activity of porous TiO_2 hollow aggregates by using a low-temperature hydrothermal method without templates.* Chemistry-A European Journal. 2007. **13**: p. 1851-5.

McKigney, E.A., et al., *Nanocomposite scitillators for radiation detection and nuclear spectroscopy.* Nuclear Instruments and Methods in Physics Research, 2007. **579**: p. 15-8.

Medintz, I. L., Uyeda, H. T., Goldman, E.R., and Mattoussi, H., *Quantum dot bioconjugates for imaging,lebelling and sensing.* Nature Materials, 2005. **4**: p. 435-46.

Meyssamy, H., et al., *Wet-Chemical synthesis of doped colloidal nanomaterials: particles and fibers of $LaPO_4$:Eu, $LaPO_4$:Ce, and $LaPO_4$:Ce,Tb.* Advanced Materials, 1999. **11**: p. 840-4.

Miyazaki, S., Ishii, K. and Nadai, T., *The use of chitin and chiosan as drug carriers.* Chemcal & Pharmaceutical Bulletion, 1981. **29**: p. 3067-9.

Miyazaki, S., et al., *Pharmaceutical application of biomedical polymers.29. Preliminary-study on film dosage form prepared from chitosan for oral-drug delivery.* Acta Pharmaceutica Nordica 1990. **2**: p. 401-6.

Muzzarelli, R., et al., *Reconstruction of parodontal tissue with chitosan.* Biomaterials, 1989. **10**: p. 598-603.

NASA Goddard Space Flight Center*, Atoms and light energy.* <http://imagine.gsfc.nasa.gov/docs/teachers/lessons/xray_spectra/background-atoms.html>

Porteanu, H.E., et al., *Optical properties of CdS/HgS/CdS quantum dot- quantum Wells structures.* Physical Status Solidi (b), 2001. **226**: p. 219.

Riwotzki, K., et al., *Liquid-phase synthesis of doped nanoparticles:Colloids of luminescing LaPO₄:Eu and CePO₄:Tb particles with a narrow particle size distribution.* Journal of Physical Chemistry B, 2001. **104**: p. 2824-8.

Varian*, Fluorescence Spectrophotometers.* <http://www.varianinc.com/cgi-bin/nav?products/spectr/fluoro/index&cid=KMOKLQQIFQ>

Stryganyuk, G., et al., *Luminescence of Ce³⁺ doped LaPO₄ nanophosphors upon Ce³⁺ 4f-5d and band-to-band excitation.* Journal of Luminescence, 2007. **128**: p. 355-60.

Stouwdam, J. W., and Veggel, F.C.J.M.Van., *Near-infrared emission of redispersible Er³⁺, Nd³⁺ and Ho³⁺ doped LaF₃ nanoparticles.* Nano Letters, 2002. **2**(7): p. 733-7.

Stouwdam, J. W., Hebbink, G. A., Huskens, J., and Veggel, F.C.J.M.Van, *Lanthanide-doped nanoparticles with excellent luminescent properties in organic media.* Chemistry of Materials, 2003. **15**: p. 4604-16.

Stouwdam, J. W., and Veggel F.C.J.M.Van, *Improvement in the luminesence properties and processability of LaF₃/Ln and LaPO₄/Ln nanoparticles by surface modification.* Langmuir, 2004. **20**: p. 11763-71.

So, P., and Dong, C.Y., *Fluorescence spectrophotometry.* Encyclopedia of Life Science, Nature Publishing Group, 2002.

Tian, Y., et al., *Coupled composite CdS-CdSe and Core-Shell types of (CdS)CdSe and (CdSe)CdS nanoparticles.* Journal of Physical Chemistry, 1996. **100**: p. 8927-39.

Valeur, B. *Molecular Fluoresence Principles and Applications*, Wiley-VCH, Weinheim, Germany, 2002.

Warren, B.E., *X- Ray Diffraction.* Dover Publications, New York, 1990.

Wang, F., Zhang, Y., Fan, X.P., and Wang, M.Q., *Facile synthesis of water-soluble LaF₃:Ln³⁺ nanocrystals.* Journal of Materials Chemistry, 2006. **16**: p. 1031-4.

Wang, F., Zhang, Y., Fan, X.P., and Wang, M.Q., *One-pot synthesis of chitosan/LaF₃: Eu³⁺ nanocrystals for bio-applications.* Nanotechnology, 2006. **17**: p. 1527-32.

Wang, J.S., et al., *One-step synthesis of highly water-soluble LaF₃:Ln³⁺ nanocrystals in methanol without using any ligands.* Nanotechnology, 2007. **18**(465606) 6pp.

Wang, Z.L., et al., *A facile synthesis and photoluminescent properties of redispersible CeF$_3$, CeF: Tb^{3+}, and CeF$_3$:Tb^{3+} /LaF$_3$ (core/shell) nanoparticles.* Chemistry of Materials, 2006. **18** (8): p. 2030-7.

Wang, Z.G., et al., *Origin of luminescence from PMMA functionalized nanoparticles.* Physics letters A 2006. **A350**: p. 252-7.

Weber, M.J., *Probabilities for radiative and nonradiative decay of Er^{3+} in LaF$_3$* Physical Review, 1967 **157**: p. 262-72.

Zhang Y., and Lu, M. H., *Labelling of silica microsphere with fluorescent lanthanide-doped LaF$_3$ nanocrystals.* Nanotechnology, 2007. **18**(275603) 5pp.

Zhou, J., et al., *Study on an antiwear and extreme pressure additive of surface coated LaF$_3$ nanoparticles in liquid paraffin.* Wear, 2001. **249**: p. 333-7.

Zhu, L., et al., *Morphological Control and Luminescent properties of CeF$_3$ Nanocrystals.* Journal of Physical Chemistry C. 2007. **111**: p. 5898-903.